*Proceedings of the*
*Annual Stability Conference*
*Structural Stability Research Council*
*Grapevine, Texas, April 18-21, 2012*

# DSM Design of Cold-Formed Steel Columns Failing Distortionally Exposed to Fire: How Relevant is the Temperature Dependence of the Material Behavior?

A. Landesmann[1], D. Camotim[2]

## Abstract

This paper presents a numerical (shell finite element) investigation aimed at assessing the performance of the current Direct Strength Method (DSM) provisions against distortional failure to estimate the ultimate strength of fixed-ended cold-formed steel lipped channel and rack-section columns (i) subjected to various uniform temperature distributions caused by fire conditions and (ii) exhibiting different room-temperature yield stresses, covering a wide distortional slenderness range. In particular, the work addresses how does the temperature-dependence of the steel material behavior, which is felt through both the (reduced) Young's modulus and nominal yield stress values, influences the quality (accuracy and safety) of the column ultimate strength predictions provided by the DSM distortional strength curve. Three different temperature-dependent steel constitutive laws are considered, namely (i) a model prescribed in part 1.2 of Eurocode 3 (EC3) and (ii) two experimentally-based analytical expressions recently reported in the literature. The DSM column ultimate strength estimates are compared with numerical distortional failure loads obtained through geometrically and physically non-linear ANSYS shell finite element analyses that incorporate critical-mode initial imperfections with small amplitudes.

## 1. Introduction

The use of cold-formed steel structures has grown steadily during recent years as they became extremely popular in different areas of the construction industry, namely (i) low rise official, residential and industrial buildings, (ii) high storage structures and (iii) roof trussed structures. Cold-formed steel offers very flexible design solutions, exhibits a high structural efficiency (strength-to-weight ratio) and has been characterized by enormous fabrication versatility and increasingly low production and erection costs.

The knowledge about the structural behavior of cold-formed steel members at room temperature has advanced considerably in the last few years and, moreover, such advances have been incorporated in design specifications at a fairly rapid rate. Since it is well known that many cold-formed steel members are prone to distortional failure, the current design specifications include provisions dealing with this collapse mode. In particular, the Direct Strength Method (DSM – *e.g.*, Schafer 2008), which has already been incorporated in the current versions of the North-American (AISI 2007), Australian/New Zealand (AS/NZS 2005) and Brazilian (ABNT 2010) specifications for cold-formed steel structures, includes specific provisions (strength curves) for the design of columns and beams against distortional failure, whose application requires only the evaluation of yield and distortional buckling loads or moments.

[1] Civil Engineering Program, COPPE, Federal University of Rio de Janeiro, Brazil. <alandes@coc.ufrj.br>
[2] Civil Eng. Dept., ICIST, Instituto Superior Técnico, Technical University of Lisbon, Portugal. <dcamotim@civil.ist.utl.pt>

However, such provisions/curves were developed for cold-formed steel members at room temperature and it is still unknown whether they can also be adopted (with or without modifications) to estimate the ultimate strength of members subjected to elevated temperatures caused by fire conditions, which alter considerably the steel constitutive law, namely its Young's modulus, yield strength and non-linearity.

Indeed, the high "section factor"[3], associated with the use of (i) high-strength steels and (ii) very slender cross-sections, is responsible for making cold-formed steel construction significantly vulnerable to fire conditions. Therefore, the application of the currently available design methods requires the extensive use of expensive fireproofing materials, aimed at protecting the steel structures from an excessive heat increase stemming from fire hazards. This requirement quite often leads to overly conservative structural designs, which are unduly uneconomical. Moreover, it is fair to say that the research activity devoted to cold-formed steel members under fire conditions was only initiated in this century and is still rather scarce, as attested by the relatively small number of available publications on the subject. Without claiming to be complete, such publications report essentially the work done by Outinen *et al.* (2000), Kaitila (2002), Feng *et al.* (2003a-d, 2004), Lee *et al.*[4] (2003), Feng & Wang (2005a,b), Chen & Young (2006, 2007a,b, 2008), Ranawaka (2006), Ranawaka & Mahendran (2009a,b, 2010), Landesmann & Camotim (2010a,b, 2011) and Shahbazian & Wang (2011a,b, 2012). Moreover, only a small fraction of the above studies addresses failures associated with the occurrence of distortional buckling, an instability phenomenon that often governs the behavior and strength of lipped members with intermediate unrestrained lengths.

### *1.1 Motivation, Objective and Scope of this Work*

Several researchers, namely Outinen & Makelainen (2002), Lee *et al.* (2003), Mecozzi & Zhao (2005), Zhao *et al*. (2005), Chen & Young (2007a), Ranawaka & Mahendran (2009a), Kankanamge & Mahendran (2011) and Wei & Jihong (2012), investigated experimentally the variation of the cold-formed steel constitutive law with the temperature, and proposed (experimentally-based) analytical expressions to model the cold-formed steel material behavior at elevated temperatures. The temperature-dependence is taken into account through reduction factors applied to the steel Young's modulus, proportional limit stress, yield stress and ultimate stress. However, there are significant discrepancies between the reductions factors proposed in the various works, which also differ from those prescribed, for fire conditions, in the current steel design codes. Furthermore, in the course of a numerical investigation on the distortional dealing with the post-buckling behavior and ultimate strength of lipped channel and rack-section columns under fire conditions, the authors (Landesmann & Camotim 2010a,b, 2011) found that, at least for the particular column geometries analyzed and temperature-dependent material models considered, the quality (accuracy and safety) of the ultimate load estimates determined with the current DSM distortional design/strength curve/expressions (at elevated temperatures) exhibited a mild dependence on the temperature. This finding provided the motivation for the present work, considers additional models to simulate the cold-formed steel material behavior at elevated temperatures and aims at contributing towards answering the following question: "how does the temperature dependence of the steel material behavior influence the quality safety of the column ultimate load estimates provided by the current DSM distortional strength design curve?".

---

[3] The heating rate of a given cross-section varies according to its dimensions, namely the so-called "section factor", which is given by *Hp*/*A* relationship, where (i) *Hp* is the steel cross-section perimeter exposed to the fire and (ii) *A* is the cross-sectional area. A larger *Hp*/*A* value corresponds to a higher susceptibility to fire effects (or, alternatively, a higher need for the use of fireproofing materials).

[4] Although Lee *et al.* (2003) reported a quite comprehensive experimental work, covering cold-formed steels sheets with *0.4-1.2 mm* thickness, Ranawaka & Mahendran (2009a) later mentioned that the furnace-temperature measuring device used by these authors overestimated the temperature – note that Mahendran co-authors both publications. Thus, because the method employed to measure the strains was inadequate, the yield stress and Young's modulus values reported, as well as the associated stress-strain curves, are most likely not accurate/reliable.

*1.2 Outline of the Paper*

The paper begins by presenting a literature survey concerning the available cold-formed steel constitutive laws at elevated temperatures caused by fire conditions, devoting particular attention to the different reductions factors proposed to model the erosion of the steel Young's modulus and yield stress. The main output of this literature review is the selection of *three* representative temperature-dependent constitutive laws to model the cold-formed steel material behavior, which will be subsequently adopted to (i) perform the distortional failure shell finite element analyses (SFEA) and (ii) determine the DSM predictions corresponding to the numerical failure loads. The next step consists performing sequences of "trial and error" buckling analyses, in order to select *two* fixed-ended column geometries (cross-section dimensions and lengths), one involving a lipped channel and the other a rack-section, that ensure distortional buckling and failure modes as "pure" as possible – *i.e.*, the selected columns exhibit distortional critical buckling loads that are significantly lower than their local and global counterparts. Then, after briefly addressing the shell finite element model employed to perform the geometrically and materially non-linear analyses in the commercial code ANSYS (SAS 2009), (i) illustrative numerical results concerning the column distortional post-buckling behavior and ultimate strength are presented and discussed, and (ii) a *parametric stud*y is carried out, in order to assemble a fairly extensive fixed-ended lipped and rack-section column numerical ultimate strength "data bank". The columns analyzed (i) display the three temperature-dependent cold-formed steel constitutive laws selected earlier, (ii) exhibit several room temperature yield stresses, covering a wide distortional slenderness range, (iii) contain critical-mode (distortional) initial geometrical imperfections with small amplitude (equal to *10%* of the wall thickness *t*), and (iv) are compressed under various uniform temperatures that may be as high as *600* ºC. Finally, after comparing the trends of the numerical column ultimate loads with those exhibited by some experimental values reported in the literature, the available (numerical and experimental) failure loads under various temperatures are used to assess the quality (accuracy and safety) of the estimates provided by the current DSM distortional strength curve. In particular, the comparison between the column ultimate loads and their DSM predictions makes it possible (i) to appraise how the current distortional strength curve is able to cope with the variation of the constitutive law variation with the temperature, for the different models, and also (ii) to suggest a few preliminary modifications/adjustments to account for the temperature effects.

## 2. Steel Constitutive Law at Elevated Temperatures – Available Models

The search for accurate methodologies to ensure the fire safety design of cold-formed steel members must begin with a fairly accurate knowledge on the variation of the cold-formed steel thermal and mechanical properties with the temperature, which may reach rather high values. Moreover, it is by now widely recognized that the reduction factors applicable to hot-rolled steel grades are not valid for the cold-formed steel ones. Indeed, as stated by Sidey & Teague (1988) quite a while ago, the strength reduction of cold-formed steels subjected to elevated temperatures may be *10-20%* higher than that experienced by hot-rolled steels, due to the different metallurgical composition and molecular surface effects. Furthermore, Kankanamge & Mahendran (2011) recently found that cold-formed steels under elevated temperatures are likely to lose the additional strength acquired during the cold-working process at ambient temperature.

Although design standards, such as BS5950-8 (1990) or EC3-1.2 (2005), contain provisions specifying the mechanical properties of cold-formed steels at elevated temperatures, they do not include accurate reduction factors for the corresponding Young's modulus and yield stress values. Indeed, BS5950-8 (i) provides no Young's modulus reduction factor (the key feature to determine the column buckling behavior), (ii) only presents yield stress reduction factors for temperatures below *600* ºC and (iii) considers proof stresses corresponding to *0.5%*, *1.5%* and *2.0%* strain levels, in contrast with the current

common practice of dealing with *0.2%* proof stresses. On the other hand, EC3-1.2 (2005) treats cold-formed steel members similarly to thin-walled (*i.e.*, class *4*) hot-rolled and welded members – the only differences, with respect to the remaining (class *1*, *2* or *3*) hot-rolled and welded members, consist of (i) the effective yield stress definition (*0.2%* proof stress), (ii) the corresponding reduction factors (given in Table E.1 of Annex E), (iii) a recommendation to neglect the load-bearing capacity of class *4* members at temperatures higher than *350* ºC and (iv) a note stating that the Young's modulus reduction factors, established for hot-rolled steels, may slightly underestimate those applicable to cold-formed steels.

In order to overcome the lack of reliable information of the variation of the mechanical properties of cold-formed steel members with the temperature, essential for their design in fire conditions, Lee *et al.* (2003), Mecozzi & Zhao (2005), Chen & Young (2007a), Ranawaka & Mahendran (2009a), Kankanamge & Mahendran (2011) and Wei & Jihong (2012) undertook experimental investigations, based on tensile coupon tests at elevated temperatures, and came up with several proposals of experimentally-based analytical expressions providing stress-strain curves to be used in the fire safety design of cold-formed steel members. The analysis of the test data showed that the cold-formed steel yield stress reduction factor is highly dependent on the strain level assumed to correspond to the measured yield stress – a conservative approach consists of adopting for design strength the reduced *0.2%* proof stress, as done in EC3-1.2 2005. In the above proposals, the temperature dependence is always taken into account by means of reduction factors applicable to the steel Young's modulus ($k_e$) and nominal yield stress ($k_y$). Figs. 1(a)-(b) make it possible to compare the temperature variations of the cold-formed steel $k_e$ and $k_y$ values prescribed by EC3-1.2 (2005) and proposed by Chen & Young (2007a) and Ranawaka & Mahendran (2009a), which are those adopted to carry out the research work reported in this paper – they are presented in some detail in the next subsections. One readily observes that there are significant discrepancies between the curves concerning the various constitutive laws – in particular, note that both EC3-1.2 reduction factors model are higher than their two counterparts for most of the considered temperature range, which is bound to influence significantly the column buckling, post-buckling and ultimate strength behaviors analyzed in this study. Fig. 1(c) illustrates the qualitative differences between the steel stress-strain curves ($\sigma_T/\sigma_{y.20}$ *vs.* $\varepsilon$, where the applied stress at a given temperature, $\sigma_T$, is normalized with respect to the room temperature yield stress $\sigma_{y.20}$) prescribed by the three models for *T=20* ºC (room temperature), *T=400* ºC and *T=600* ºC. Note that, regardless of the material model considered, the non-linearity of the steel stress-strain curve increases substantially with the temperature (for *T=20* ºC, the EC3-1.2 model prescribes a bi-linear constitutive law, corresponding to an elastic-perfectly plastic material).

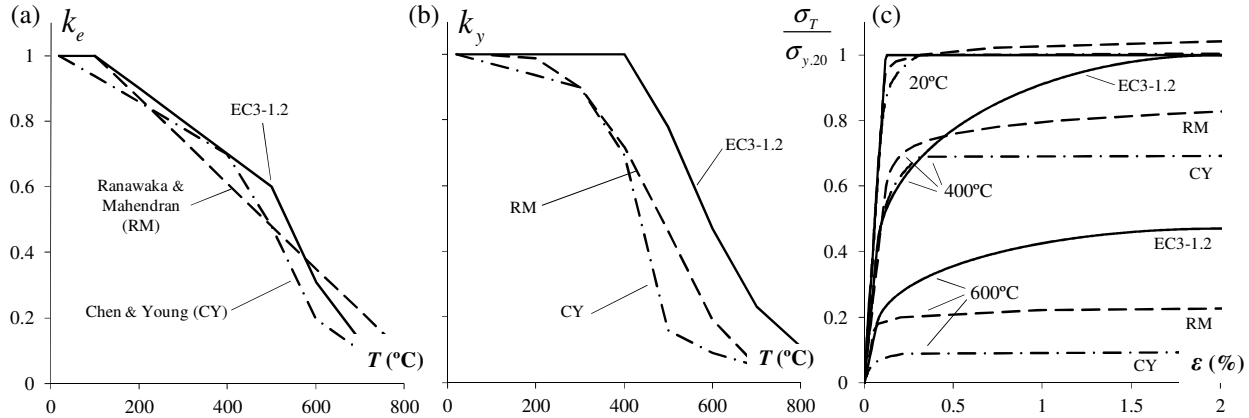


**Figure 1.** Variation of (a) $k_e$ and (b) $k_y$ with the temperature ($T \leq 800$ºC), and (c) cold-formed steel constitutive laws according to EC3-1.2 (2005), Chen & Young (2007a) and Ranawaka & Mahendran (2009a), for *T=20-400-600* ºC ($\varepsilon \leq 2\%$).

*2.1 Eurocode 3 Part-1.2 Model*

Part 1.2 of Eurocode 3 (EC3-1.2 2005) provides analytical expressions to define the steel constitutive law at elevated temperatures, which are based on the work of Kirby & Preston (1988) on hot-rolled steels and, thus, may not model accurately the cold-formed steel material behavior at elevated temperatures. The effect of creep is implicitly considered and the material models are applicable for heating between *2* and *50 K/min*. The corresponding stress-strain curve, given by

$$\sigma_T = \begin{cases} \varepsilon \cdot E_T & \text{for } \varepsilon \le \varepsilon_{p.T} \\ \sigma_{p.T} - c + (b/a)\left[a^2 - \left(\varepsilon_{y.T} - \varepsilon\right)^2\right]^{0.5} & \text{for } \varepsilon_{p.T} < \varepsilon < \varepsilon_{y.T} \\ \sigma_{y.T} & \text{for } \varepsilon_{y.T} \le \varepsilon \le \varepsilon_{u.T} \end{cases} \quad (1)$$

$$a^2 = \left(\varepsilon_{y.T} - \varepsilon_{p.T}\right)\left(\varepsilon_{y.T} - \varepsilon_{p.T} + c/E_T\right),\ b^2 = c\left(\varepsilon_{y.T} - \varepsilon_{p.T}\right)E_T + c^2,$$

$$c = \frac{\left(\sigma_{y.T} - \sigma_{p.T}\right)^2}{\left(\varepsilon_{y.T} - \varepsilon_{p.T}\right)E_T - 2\left(\sigma_{y.T} - \sigma_{p.T}\right)},$$

is divided into three different regions, associated with distinct strain ranges[5]. Notice that the stress-strain curve shape is considerably influenced by the temperature and proportionality limit strain ($\varepsilon_{p.T}=\sigma_{p.T}/E_T$). The initial part of the well-defined yield plateau exhibited by the $T=20$ °C curve is replaced by a strain-hardening region that becomes more pronounced as the temperature increases. The stress-strain curve (i) is linear elastic, with slope $E_T$, up to the proportional limit $\sigma_{p.T}$, then (ii) becomes elliptic in the region associated with the transition between the elastic and plastic ranges, up to the effective yield stress $\sigma_{y.T}$ (corresponding to $\varepsilon_{y.T}=0.02$), and (iii) ends with perfectly flat yield plateau up to a limit strain $\varepsilon_{u.T}=0.15$.[6]

*2.2 Chen & Young Model*

The experimentally-based constitutive model proposed by Chen & Young (2007a) exhibits a Ramberg-Osgood (1943) format, previously adopted by Mirambell & Real (2000) and Rasmussen (2003) to describe the stainless steel constitutive law at room temperature. This means that the corresponding temperature-dependent equations, given by

$$\varepsilon_T = \begin{cases} \dfrac{\sigma_T}{E_T} + 0.002\left(\dfrac{\sigma_T}{\sigma_{y.T}}\right)^{n_T} & \text{for } \sigma_T \le \sigma_{y.T} \\ \dfrac{\sigma_T - \sigma_{y.T}}{E_{y.T}} + \varepsilon_{u.T}\left(\dfrac{\sigma_T - \sigma_{y.T}}{\sigma_{u.T} - \sigma_{y.T}}\right)^{m_T} + \varepsilon_{y.T} & \text{for } \sigma_T > \sigma_{y.T} \end{cases} \quad (2)$$

express the strain in terms of the stress through by means of a two-part curve with a continuous derivative at the transition point, occurring for $\sigma_T=\sigma_{y.T}$ ($\sigma_T$ is the applied stress at temperature $T$), where $E_T$ and $\sigma_{y.T}$ are the initial Young's modulus and effective yield stress, associated with the "elastic" limit strain $\varepsilon_{y.T}$. The constitutive law temperature-dependence is felt through various quantities, obtained from the expressions

[5] Although the EC3-1.2 (2005) model further extends the stress-strain relationship, to include strain-hardening, for steel temperatures below 400 °C (this strain-hardening is negligible for temperatures higher than 400 ºC), this effect is not considered in the present work.

[6] The $\sigma_{p.T}$, $\sigma_{y.T}$ and $E_T$ values depend on the temperature $T$ and are tabulated in EC3-1.2 (2005).

$$E_{y.T}=\frac{E_T}{1+0.002\cdot n_T\left(E_T/\sigma_{y.T}\right)},\ n_T=20-0.6\sqrt{T},\ \ m_T=1+T/350,\ \frac{\varepsilon_{u.T}}{\varepsilon_{u.20}}=0.2-\frac{(T-1000)^6}{-1.1\cdot 10^{18}},$$

$$\frac{\sigma_{u.T}}{\sigma_{u.20}}=\begin{cases}1-\dfrac{(T-22)^6}{1.5\cdot 10^4} & \text{for } 20\le T\le 320\ ^\circ C\\ 0.026-\dfrac{(T-1000)^4}{-2.24\cdot 10^{11}} & \text{for } 320<T\le 1000\ ^\circ C\end{cases},$$

where (i) $E_{y.T}$ is the inverse strain-stress slope at the transition point curve and (ii) the calibration of the constants appearing in the various expressions was based on the tensile coupon test results. The test program included the steel grades *G550* and *G450*, with nominal yield stresses equal to *550 MPa* and *450 MPa*, and the plate thicknesses of the coupon test specimens were equal to *1.0 mm* and *1.9 mm*. Both steady state and transient tests were conducted at various temperatures, up to *1000*°C.

*2.3 Ranawaka & Mahendran Model*

Ranawaka & Mahendran (2009a) performed an extensive experimental program comprising the testing of tensile coupons (i) with three nominal thicknesses (*0.60-0.80-0.95* mm, (ii) made of steel grades *G550* and *G250*, with nominal yield stresses equal to *550 MPa* and *250 MPa*, and (iii) subjected to eight uniform temperatures (*20-100-200-350-500-600-650-800*°C). The output of this experimental program was also a Ramberg-Osgood type constitutive model, according to which $\varepsilon_T$ is given by the expression

$$\varepsilon_T=\frac{\sigma_T}{E_T}+\beta\left(\frac{\sigma_{y.T}}{E_T}\right)\left(\frac{\sigma_T}{E_T}\right)^{\eta_T}\quad,\ (3)$$

where $\beta$=*0.86* (value also adopted by Outinen 1999) and the variation of $\eta_T$ with the temperature is given, for the steel *G550* (model adopted in this work for all steel grades), by

$$\eta_T=-3.05\cdot 10^{-7}T^3+0.0005\cdot T^3-0.2615\cdot T+62.653\quad \text{for } 20\le T\le 800\ ^\circ C\quad .\ (4)$$

Out of the various analytical expressions developed by Ranawaka & Mahendran (2009a) to quantify the temperature-dependence of their constitutive law, those used in this work concern the variation of the Young's modulus and yield stress with the temperature *T*, which read

$$\frac{E_T}{E}=\begin{cases}1 & \text{for } 20\le T\le 100\ ^\circ C\\ -0.0013T+1.1297 & \text{for } 100<T\le 800\ ^\circ C\end{cases}\quad (5)$$

$$\frac{\sigma_{y.T}}{\sigma_{y.20}}=1.8476\cdot 10^{-11}T^{3.98}-1.91\cdot 10^{-8}T^3+3.625\cdot 10^{-6}T^{1.997}+0.99\quad \text{for } 20\le T\le 800\ ^\circ C\quad .\ (6)$$

## 3. Column Geometry Selection – Buckling Behavior

The cold-formed steel fixed-ended (end sections locally and globally fixed with warping prevented) lipped channel and rack-section columns analyzed in this work exhibit the cross-section dimensions and elastic constants given in Table 1. These cross-section dimensions make it possible to select column lengths ensuring pure distortional critical buckling modes. The buckling analyses required to identify the

above column geometries were carried out in the code GBTUL (Bebiano *et al.* 2008a,b), which is based on Generalized Beam Theory (GBT). The curves depicted in Fig. 2 provide the variation of the elastic critical buckling stress $\sigma_{cr}$, normalized with respect to the room temperature critical distortional) buckling stress $\sigma_{cr.D.20}$, with the column length $L$ (logarithmic scale) and temperature $T$ for the lipped channel and rack-section columns – *3* temperatures are considered (room temperature *20*ºC, *400*ºC and *600*ºC) and the EC3-1.2 constitutive model is adopted. Also shown are the critical (distortional) buckling mode shapes of the two column sets analyzed, which correspond to $L_D$=*132 cm* (lipped channel) and $L_D$=*242 cm* (rack-section). Note that (i) any given buckling curve can be obtained through a "vertical translation" of the top one, with a magnitude that depends exclusively on the Young's modulus erosion stemming from the rising temperature (Poisson's ratio υ is deemed temperature-independent and equal to *0.3*)[7], and that (ii) the critical distortional stress ($\sigma_{cr.D.T}$) corresponds to the same length ($L_D$) for each column cross-section.

**Table 1.** Column cross-section dimensions, elastic constants, lengths and critical stresses.

| Column | $b_1$ (mm) | $b_2$ (mm) | $b_3$ (mm) | $b_4$ (mm) | $t$ (mm) |
|---|---|---|---|---|---|
| Rack | 134.7 | 80.8 | 24.2 | 47.1 | 2.3 |
| Lipped C | 130 | 100 | 12.5 | -- | 2.0 |

| Column | $E$ (GPa) | $L_D$ (cm) | $\sigma_{cr.D.20}$ (MPa) |
|---|---|---|---|
| Rack | 210 | 242 | 253.7 |
| Lipped C | 205 | 132 | 191.5 |

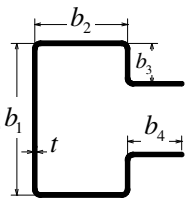


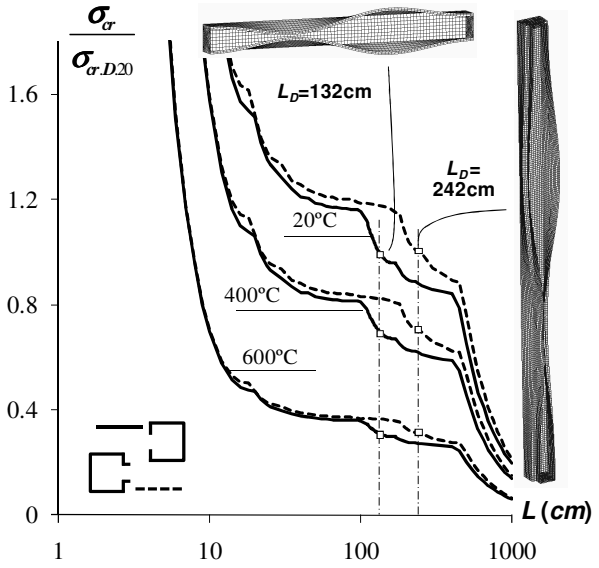


**Figure 2.** Variation of the buckling curve $\sigma_{cr}/\sigma_{cr.D.20}$ *vs. L* with *T* for the selected columns (EC3-1.2 model).

## 4. Column Post-Buckling Behavior and Ultimate Strength

After briefly addressing the SFE model employed to perform the geometrically and materially non-linear analyses, numerical results concerning the influence of the steel constitutive law adopted on the column distortional post-buckling behavior and strength are presented and discussed.

### *4.1 Numerical Model*

The column distortional post-buckling analyses were carried out in the code ANSYS (2009), employing a shell finite element model previously validated by the authors (Landesmann & Camotim 2010a,b, 2011) that involves column discretizations into fine SHELL181 (ANSYS nomenclature) element meshes – *4*-node shear deformable thin-shell elements with *six* degrees of freedom per node and full integration. Both the residual stresses and corner effects were neglected. The analyses (i) were performed by means of an incremental-iterative technique combining Newton-Raphson's method with an arc-length control strategy and (ii) simulate the response of columns subjected to a uniform temperature distribution (*i.e.*, they are

[7] Naturally, the Young's modulus reduction factor $k_e$, whose variation with the temperature $T$ is illustrated in Fig. 1(a), makes it possible to quantify the decrease in the column critical buckling load $P_{cr.T}$ associated with a given length.

deemed engulfed in flames and, thus, share the surrounding air temperature – Landesmann *et al.* 2009) and subsequently axially compressed up to failure – steady state analyses providing failure loads[8].

The columns analyzed contained initial geometrical imperfections with a critical-mode (distortional) shape and amplitude equal to *10%* of the wall thickness *t*. Due to the column distortional post-buckling asymmetry, these initial imperfections involve outward (lipped channel columns) and inward (rack-section columns) flange-lip motions – those leading to lower post-buckling strengths (*e.g.*, Prola & Camotim 2002a,b)[9]. Each critical buckling mode shape was determined by means of an ANSYS buckling analysis, performed with exactly the same shell finite element mesh employed to carry out the subsequent non-linear (post-buckling) analysis – this procedure makes it very easy to "transform" the buckling analysis output into a non-linear analysis input. The column end sections were fixed, a support condition modeled by means of rigid end-plates attached to the end cross-section centroids and only allowed to exhibit axial translations. Finally, the axial compression was applied by means of two point loads acting on the end-plate points corresponding to the cross-section centroids. Those forces are applied in small increments, by means of the ANSYS automatic load stepping procedure.

The multi-linear stress-strain curve available in ANSYS code is adopted to model the steel material behavior. Its first branch models the linear elastic range, up to the proportional limit stress and with a slope equal to Young's modulus. The following branches stand for the inelastic range, which accounts for (kinematic) strain-hardening. Finally, note that, since the distortional post-buckling analyses carried out involve large inelastic strains, the nominal (engineering) static stress-strain curve is replaced by a relation between the true stress and the logarithmic plastic strain. The variation of the cold-formed steel material behavior with the temperature is described by three constitutive models, namely (i) that prescribed in EC3-1.2 (2005) and (ii) the experimentally-based ones analytical proposed by Chen & Young (2007a) and Ranawaka & Mahendran (2009a), all previously described in subsections 2.1-2.3 of this paper.

*4.2 Elastic-Plastic Post-Buckling Behavior– Ultimate Strength*

Attention now is devoted to the qualitative and quantitative influence of the temperature-dependent steel constitutive law on the column elastic-plastic distortional post-buckling and ultimate strength behaviors. Fig. (3) shows a sample of the geometrically and materially non-linear equilibrium paths $P/P_{cr.20}$ *vs.* $|\delta|/t$[10], determined to obtain the ultimate loads $P_{u.T}$ (identified by white circles). As for Fig. (4), it shows the von Mises stress distributions occurring at the distortional collapse ($P=P_{u.D.T}$). Both figure concern analyses of lipped channel and rack-section columns made of steel with $\sigma_{y.20}=550\,MPa$ steel (room temperature yield stress) and subjected to temperatures $T=20/100\text{-}400\text{-}600$ºC – the EC3-1.2 model for a temperature-dependent constitutive law was adopted. The observation of these elastic-plastic distortional post-buckling and ultimate strength results prompt the following remarks:

(i) Obviously, the ultimate strength decreases as the temperature *T* rises for all columns.

(ii) As expected, regardless of the cross-section shape and temperature, the $P_u/P_{cr.20}$ curves concerning the EC3-1.2 model columns are consistently above those stemming from the two experimentally-

[8] At this stage, it is worth noting that the authors (Landesmann & Camotim 2010a,b) have shown that the failure loads yielded by the steady state analyses match the more realistic failure temperatures obtained through the "corresponding" transient analyses (axially compressed columns heated up to failure), which means that the column (distortional) failure under fire conditions can be fully investigated by resorting only to failure loads.

[9] Obviously, the distinction between distortional initial gometrical imperfections involving inward and outward flange-lip motions is only relevant in column buckling in modes exhibiting odd half-wave numbers.

[10] These equilibrium paths relate the applied load, normalized value with respect to the corresponding column critical buckling load $P_{cr.D}$, to the normalized displacement ratio $|\delta|/t$, where $|\delta|$ is the absolute value of the maximum vertical displacement occurring along the flange-stiffener longitudinal edges and *t* is the wall thickness.

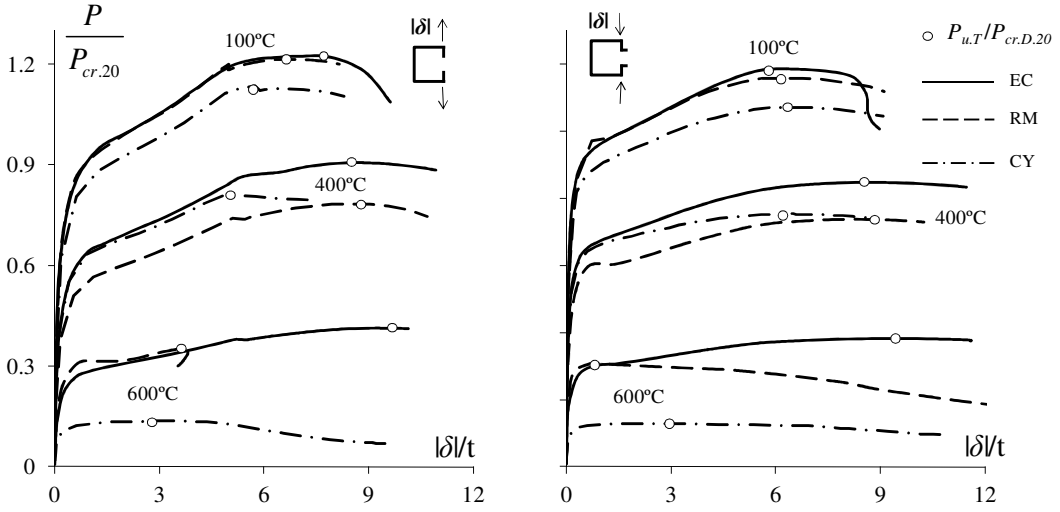


**Figure 3.** Lipped channel and rack-section column distortional post-buckling equilibrium paths for $\sigma_{y.20}$=*550MPa*, temperatures *T=100-400-600*ºC and the constitutive models of EC3-1.2, Chen & Young (2007a) and Ranawaka & Mahendran (2009a).

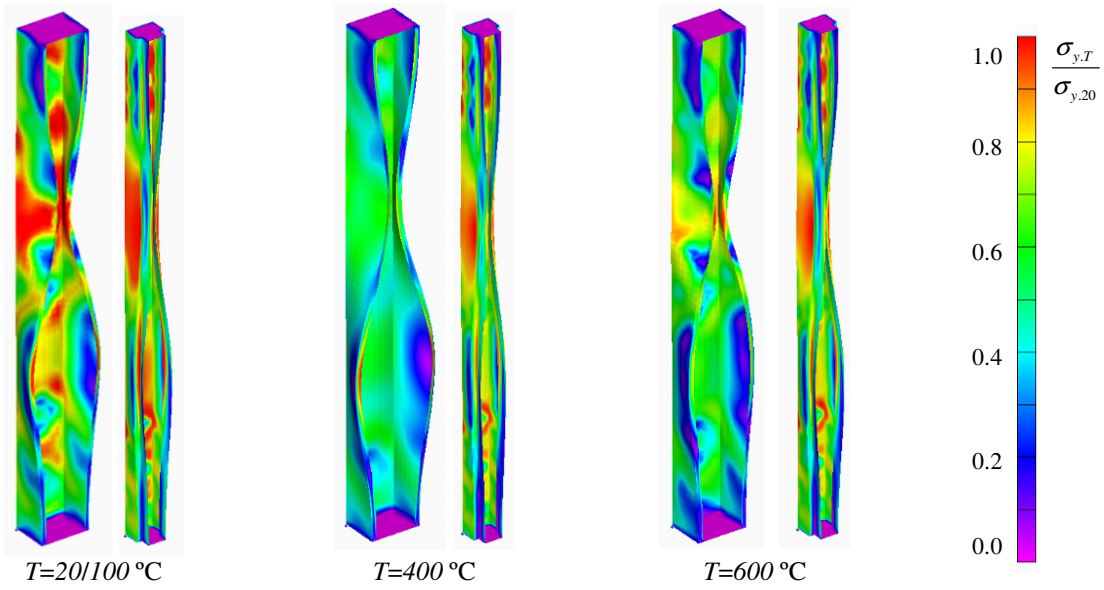


**Figure 4.** Lipped channel and rack-section column von Mises stress distributions at distortional collapse for $\sigma_{y.20}$=*550 MPa*, temperatures *T=100-400-600*ºC and the constitutive model prescribed by EC3-1.2.

based constitutive models. This is just a direct consequence from the lower Young's modulus and yield stress reduction factors prescribed by this constitutive model – see Figs. 1(a)-(b).

(iii) Regardless of the temperature and constitutive model, the $P_u/P_{cr.20}$ values concerning the lipped channel columns are consistently higher than their rack-section column counterparts.

(iv) For all the column sets analyzed, the $P_u/P_{cr.D}$ values are always ordered according to the constitutive model sequence EC (EC3-1.2), RM (Ranawaka & Mahendran) and CY (Chen & Young), with one exception: the columns subjected to *T=400*ºC, for which the sequence is EC, CY and RM. This is due to the fact that, for this particular temperature, there is a reduction factor $k_y$ inversion for the RM and CY constitutive models – see Fig. 1(b). In other words, the $P_u/P_{cr.D}$ values follow the trend of the yield stress reduction factor – this confirms the high relevance of the influence of the yield stress reduction factor on the column post-buckling behavior.

(v) Since the thermal action effects are negligible (uniform temperature and "free-to-deform" columns), the distortional failure modes are virtually identical in the three column pairs, *i.e.*, they do not depend on the temperature. Moreover, the von Mises stress distributions are also qualitatively rather similar – the higher stresses always occur in the vicinity of the lip free ends. It is worth noting that the collapse is always triggered by the yielding of the web-flange edge regions in the vicinity of the half-wave central regions. Quantitatively speaking, the stress values obviously decrease as the temperature rises and continuously erodes the steel material behavior.

(vi) Finally, it should be mentioned that no clear trend has been detected concerning the influence of the temperature on the amount of column elastic-plastic strength reserve and ductility prior to failure.

## 4. Parametric Study

This section presents and discusses the results of the parametric study carried out to gather ultimate strength data that will make it possible to assess the DSM estimates. This parametric study involved a total of *252* columns, corresponding to all possible combinations of the (i) two fixed cold-formed column geometries defined in Table 1 (lipped channel and rack-section), (ii) three constitutive models described in section 2 (EC, CY and RM), (iii) seven uniform temperatures (*T=20-100-200-300-400-500-600 ºC)* and, (iv) six steel grades, with room temperature yield stresses $\sigma_{y.20}$*=250-355-550-700-1000-1200 MPa* – these values were selected to cover wide distortional slenderness ranges for all column sets: $\bar{\lambda}_{D.T}$ varies from *0.99* to *3.56* (EC model), *0.57* to *2.69* (CY model) and *0.74* to *2.76* (RM model).

### *4.1 Numerical Ultimate Strengths*

Tables A1 to A7, presented in Annex, contain (i) all the numerical column ultimate loads ($P_{u.T}$) obtained, normalized with respect to the corresponding squash loads ($P_{y.T}=Af_{y.T}$), and (ii) the associated distortional slenderness values ($\bar{\lambda}_{D.T}$). Those seven ultimate load sets (one for each temperature) are also plotted in Figs. 5(a)-(b) and 6, respectively for room (*T=20 ºC*) and elevated (*T=100-200-300-400-500-600 ºC*) temperatures, together with a number of available experimental results reported (i) in Schafer's state-of-the-art report (Schafer 2008), for *T=20 ºC*, and (ii) by Ranawaka (2006), for elevated temperatures[11]. The observation of these eight plots makes it possible to conclude that:

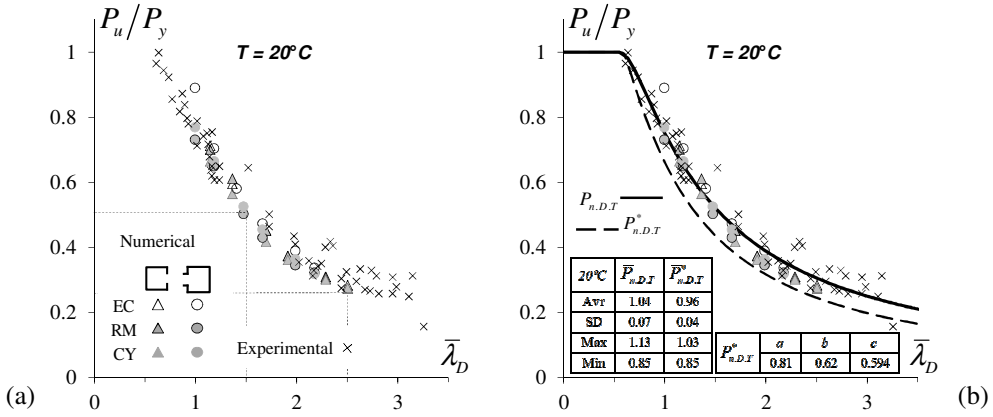


**Figure 5.** (a) Numerical and experimental (Schafer 2008) room temperature ultimate load ratios $P_u/P_{cr.D}$ plotted against the column distortional slenderness $\bar{\lambda}_D$, and (b) comparison with the current and modified DSM distortional strength curves.

[11] The results reported by Ranawaka (2006) concern the following column dimensions and room temperature yield stresses: (i) $b_1$*=30, $b_2$=30, $b_3$=5, t=0.60 mm,* $\sigma_{y.20}$*=315-675 MPa* and *L=20 cm* (lipped channel columns) and (ii) $b_1$*=40, $b_2$=30, $b_3$=5, $b_4$=10, t=0.60-0.80-0.95 mm,* $\sigma_{y.20}$*=250-550 MPa* and *L=22-24-28 cm* (rack-section columns).

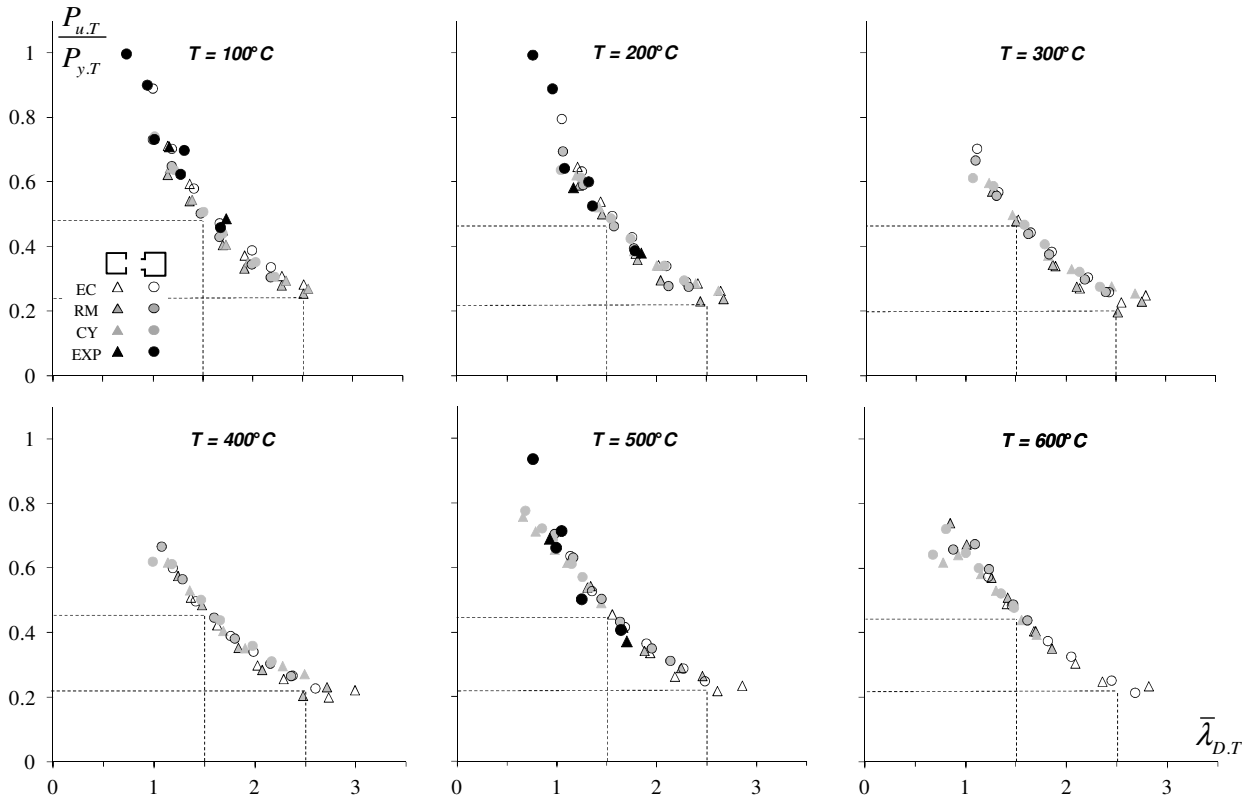


**Figure 6.** Numerical and experimental (Ranawaka 2006) ultimate load ratios $P_{u.T}/P_{cr.T}$ plotted against the column distortional slenderness $\bar{\lambda}_{D.T}$ for elevated temperatures.

(i) As it would be logical to anticipate, the four $P_{u.T}/P_{y.T}$ *vs.* $\bar{\lambda}_{D.T}$ "clouds" follow trends that can be accurately described by "Winter-type" strength/design curves. Moreover, the "vertical dispersion" is acceptable in all of them, even if the stocky columns subjected to $T=600$ ºC and analyzed with the CY constitutive model exhibit considerably lower ultimate loads, due to more significant reduction factors – recall that this model stipulates a yield stress reduction factor sudden drop for $T\geq500$ºC[12].

(ii) It is clear that the $P_{u.T}/P_{y.T}$ values of the columns at room temperature (or subjected to $T=100$ºC) are above those concerning columns subjected to elevated temperatures ($T>100$ºC). The (dashed) grid lines included in Figs. 5(a) and 6, associated with $\bar{\lambda}_{D.T}=1.5$ and $\bar{\lambda}_{D.T}=2.5$, provide a good visualization of this assertion – the room temperature column horizontal lines lie visibly above those concerning their elevated temperature column counterparts, which are located roughly at the same level.

(iii) The experimental results plotted in Figs. 5(a) ($T=20$ºC) and 6 ($T=100$-$200$-$500$ºC) are well "mingled" with the numerical values and, moreover, follow exactly the same trend ("Winter-type curve").

## 5. DSM Design Considerations

This section addresses the adequacy of the current Direct Strength Method (DSM) distortional strength curve to predict the ultimate strength of the cold-formed steel lipped channel and rack-section columns analyzed in this work, which (i) fail distortionally at elevated temperatures and (ii) exhibit three different

[12] Both the RM and CY constitutive models adopted in this work are based on high-strength steel (*G550*) parameters. However, it should be pointed out that there is a considerable difference in yield stress erosion between low- and high-strength steels in the *200-500* ºC range. For instance, for $T>400$ºC, the high-strength steels lose their strength more rapidly than the low-strength ones, due to the more significant amount of cold-working (Ranawaka & Mahendran 2009a).

temperature-dependent steel constitutive laws – in particular, it is intended to assess whether the quality of the DSM ultimate load estimates is affected by this temperature-dependence. It is worth noting that the DSM was (i) originally developed (Schafer & Peköz 1998), (ii) subsequently improved (Schafer 2008) and (iii) included in the current version of the North American specification for cold-formed steel structures (NAS 2007), but always in the context of room temperature. In this context, the nominal ultimate load of cold-formed steel columns failing in distortional modes is given by the expressions

$$P_{n.D} = \begin{cases} P_y & \text{for } \bar{\lambda}_D \leq 0.561 \\ P_y \left[ 1 - 0.25 \left( P_{cr.D} / P_y \right)^{0.6} \right] \left( P_{cr.D} / P_y \right)^{0.6} & \text{for } \bar{\lambda}_D > 0.561 \end{cases} , \quad (7)$$

where (i) $P_{cr.D}$ and $P_y$ are the column (distortional) critical buckling squash loads and (ii) the column distortional slenderness is given $\bar{\lambda}_D = (P_y / P_{cr.D})^{0.5}$.

The approach followed in this work, which was already (partially) explored by other researchers, namely Chen & Young (2006, 2007b, 2008), Ranawaka & Mahendran (2009b) and Landesmann & Camotim 2010a,b, 2011), consists of modifying Eq.(7) in order to account for the influence of the temperature on $P_{cr.D}$ and $P_y$. This influence is felt through the Young's modulus and yield stress values, which are progressively reduced as the temperature (caused by the fire conditions) increases. In other words, $P_{cr.D}$ and $P_y$ (or $\sigma_y$) are replaced by $P_{cr.D.T}$ and $P_{y.T}$ (or $\sigma_{y.T}$) – note that this implies that $\bar{\lambda}_D$ also varies with $T$.

Figs. 5(b) ($T=20$ºC) and 7 (elevated temperatures) compare the current DSM distortional strength curve (solid line) with (i) the numerical ultimate loads obtained in this work and (ii) the experimental failure loads reported by Schafer (2008), for $T=20$ºC, and Ranawaka (2006), for $T=100\text{-}200\text{-}500$ºC. Each plot in Fig. 7 concerns a different temperature and the numerical ultimate loads correspond to (i) the lipped channel and rack-section column geometries selected, (ii) three temperature-dependent constitutive models and (iii) six room temperature yield stresses ($\sigma_{y.20}=250\text{-}355\text{-}550\text{-}700\text{-}1000\text{-}1200\,MPa$). Figs. 8(a) ($T=20$ºC) and 9 (elevated temperatures), on the other hand, show the corresponding $P_{n.D.T}/P_{u.T}$ *vs.* $\bar{\lambda}_{D.T}$ plots (the numerical values are given in Tables A1 to A7), thus providing pictorial representations of the quality (accuracy and safety) of the current DSM distortional ultimate strength estimates. The observation of the results presented in these seven pairs of figures prompts the following remarks:

(i) At room temperature ($T=20$ºC – Fig. 5(b)), the current DSM strength curve naturally provides accurate and mostly safe predictions of the experimental failure loads reported by Schafer (2008) – indeed, these experimental failure loads are those used to calibrate the design curve (Schafer 2000, 2005). Concerning the numerical ultimate loads, the DSM estimates are ($i_1$) safe and accurate for $\bar{\lambda}_D \leq 1.5$ and ($i_2$) unsafe (but still fairly accurate) in the higher slenderness range – the overestimation tends to grow as $\bar{\lambda}_D$ increases. These assertions are reflected in the average, standard deviation, and maximum/minimum values of the numerical $P_{n.D}/P_u$ ratios: *1.04*, *0.07* and *1.13/0.85*.

(ii) At elevated temperatures, the (modified) DSM ultimate strength predictions of the experimental failure loads reported by Ranawaka (2006) are ($ii_1$) safe and fairly accurate for $T=100$ºC, ($ii_2$) slightly unsafe for $T=200$ºC and ($ii_3$) more unsafe for $T=500$ºC (particularly if $\bar{\lambda}_D$ is high) – in the last case, the experimental $P_{u.D.T}/P_{y.T}$ values "mingle" quite well with the numerical ones. Concerning the numerical ultimate loads, the DSM estimates are ($ii_1$) slightly unsafe for $\bar{\lambda}_D \leq 1.5$ and $T<400$ºC and ($ii_2$) become progressively more unsafe as $\bar{\lambda}_D$ and/or $T$ increase. In particular, it worth noting that a few stocky columns analyzed with the CY model at high temperatures ($T=500\text{-}600$ºC) are extremely unsafe, which is due to the very pronounced yield stress drop occurring for $T \geq 500$ºC.

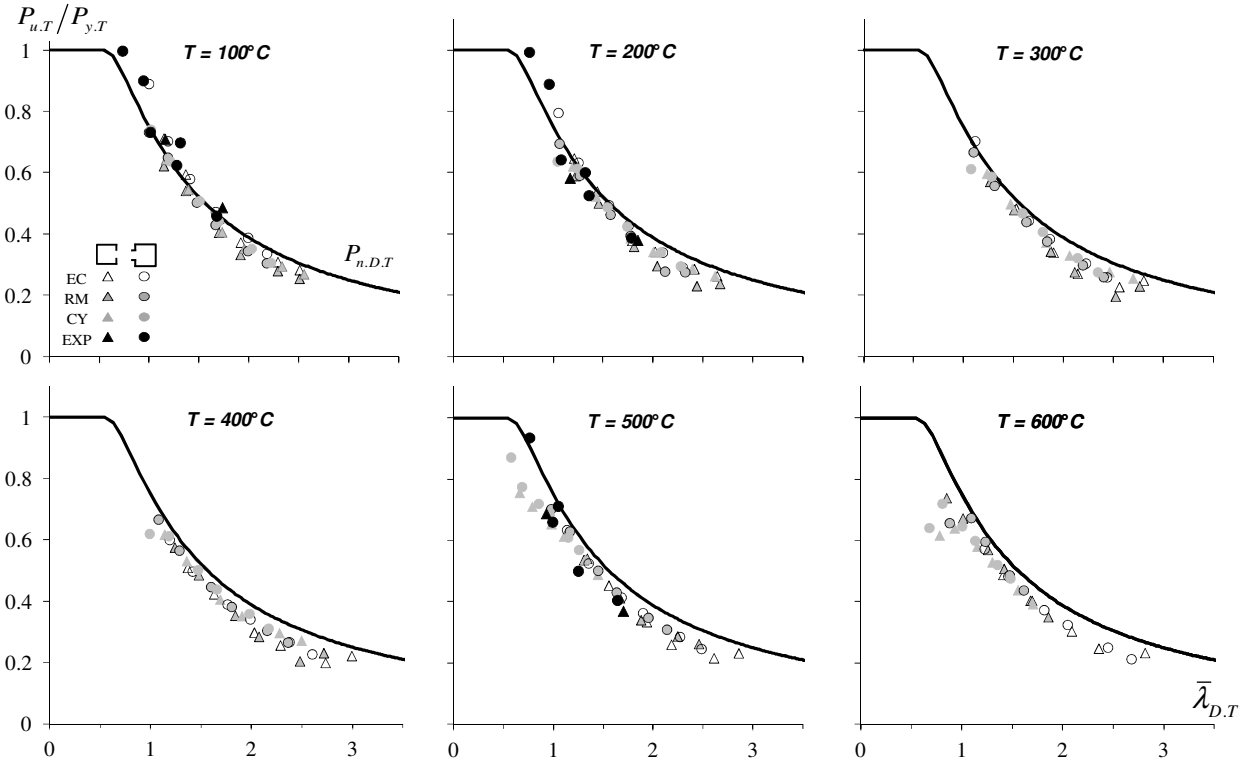


**Figure 7.** Comparison between the current DSM distortional curve and the column ultimate loads at elevated temperatures.

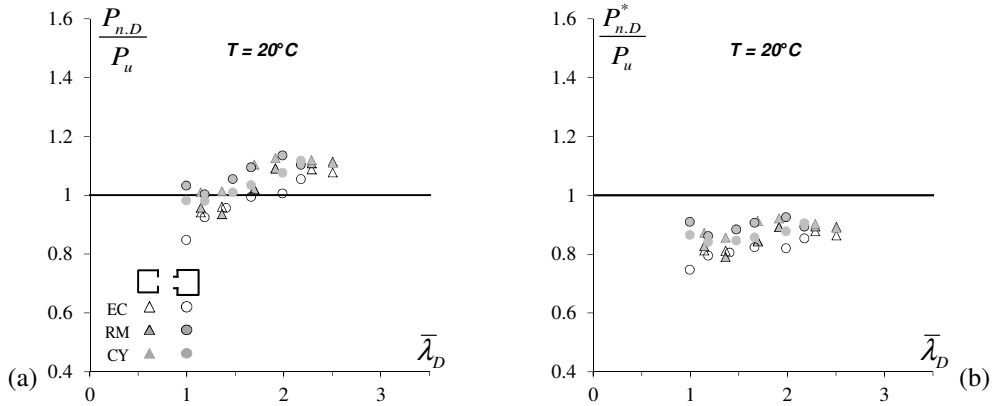


**Figure 8.** $P_{n.D}/P_u$ and $P^*_{n.D}/P_u$ ratios plotted against the distortional slenderness $\bar{\lambda}_D$ at room temperature ($T$=*20*ºC).

(iii) At room temperature, there is only one "misaligned" value ($P_u/P_y$=*0.89*), which corresponds to a stocky ($\bar{\lambda}_D$=*0.99*) rack-section column analyzed with the EC constitutive model – the $P_u/P_y$ values obtained for that same column with the RM and CY models are considerably lower: *0.73* and *0.77*, respectively. No obvious explanation could be found for this significant (and quite surprising) discrepancy, which must be due to a combination of several factors, namely (iii$_1$) $\bar{\lambda}_D \approx$*1.00* (practically coincident buckling and squash loads), (iii$_2$) the rather small initial imperfection amplitude and (iii$_3$) the non-negligible differences separating the stress-strain laws prescribed by the three constitutive models in the close vicinity of the transition between the elastic and plastic ranges – see Fig. 1(c).

(iv) Neither the cross-section shape nor the temperature-dependent constitutive model adopted seem to influence visibly the $P_{n.D.T}/P_{u.T}$ "distributions" (columns at elevated temperatures) displayed in Fig. 9 (values given in Tables A2 to A7), whose averages, standard deviations and maximum/minimum

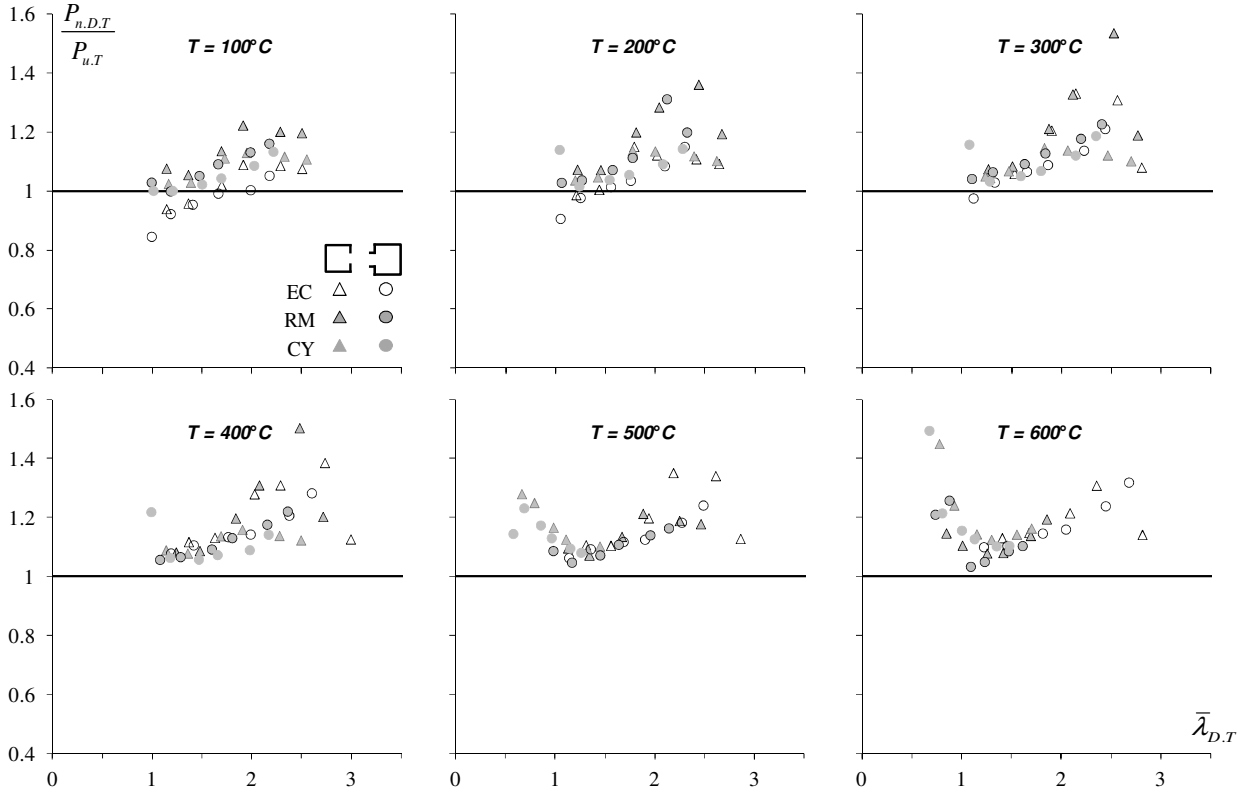


**Figure 9.** $P_{n.D.T}/P_{u.T}$ ratios plotted against the distortional slenderness $\bar{\lambda}_{D.T}$ for the six elevated temperatures.

values are presented in Fig. 10 (in this figure, $P_{n.D.T}$ stands for $P_{n.D.T}/P_{u.T}$). However, there are two exceptions to the above statement, which concern the ($iv_1$) very high $P_{n.D.T}/P_{u.T}$ values associated with the stocky columns analyzed with the CY model at *T=500-600*ºC, and ($iv_2$) low $P_{n.D.T}/P_{u.T}$ values exhibited by the stocky columns analyzed with the EC3-1.2 model at *T=100-200*ºC.

(v) The above comparisons show that ($v_1$) the current (modified) DSM distortional strength curve overestimates the vast majority of numerical column ultimate loads analyzed at elevated temperature, regardless of the temperature-dependent constitutive model adopted, and ($v_2$) the various "clouds" of $P_{u.D.T}/P_{y.T}$ values remain fairly well "aligned" with Winter-type curves. These facts suggest that it a better correlation with the numerical column ultimate loads determined in this work can be obtained by modifying Eq.(7). Therefore, the results of the limited parametric study carried out are used next to make a (preliminary) design proposal, which consists of incorporating temperature-dependent parameters into the current DSM distortional design curve, thus making it possible be to predict adequately the ultimate strength of columns at elevated temperatures.

### *5.1 Alternative DSM Distortional Strength Curve for Elevated Temperatures*

On the basis of the ultimate strength data gathered in the limited parametric study presented in section 4, a first attempt was made to find a unified DSM design approach aimed at predicting efficiently (safely and economically) the numerical failure loads concerning the columns analyzed at all temperature values. The outcome of this effort is the alternative DSM distortional design curve defined by the expressions

$$P^{*}_{n.D.T} = \begin{cases} P_{y.T} & \text{for } \bar{\lambda}_{D.T} \le c \\ P_{y.T}\left[a - 0.15\left(P_{cr.D.T}/P_{y.T}\right)^{b}\right]\left(P_{cr.D.T}/P_{y.T}\right)^{b} & \text{for } \bar{\lambda}_{D.T} > c \end{cases} , \quad (8)$$

which was obtained by modifying Eq. (7) as follows: (i) the coefficient *0.25* was replaced by *0.15* and (ii) three (slightly) temperature-dependent parameters (*a*, *b* and *c*) were incorporated, replacing the coefficient *1*, the power *0.6* and the transition distortional value *0.561*, respectively. The following sets of parameter values ensure mostly safe (but not excessively so) DSM failure load estimates for all the temperatures (including *T=20*ºC) considered in this work, as can be attested by looking at Figs. 10 and 11:

(i) $a=0.81$, for $T\leq 300$ºC, and $a=0.79$, for $T>300$ºC.

(ii) $b=0.62$, for $T\leq 300$ºC, and $b=0.66$, for $T>300$ºC.

(iii) $c=0.594$, for $T\leq 300$ºC, and $b=0.567$, for $T>300$ºC.

Figs. 5(b) (*T=20*ºC) and 10 (*T≥100*ºC) (i) compare the proposed DSM distortional strength curves with (i) the numerical and experimental column ultimate loads addressed earlier and (ii) the current DSM design curve, defined in Eq. (7). Moreover, these figures also include, in tabular form, (i) the *a*, *b*, *c* values and (ii) the averages, standard deviations and maximum/minimum exhibited by the ratios $P^{*}_{n.D.T}/P_{u.T}$, where $P^{*}_{n.D.T}$ are the ultimate strength predictions provided by Eq. (8) – all $P^{*}_{n.D.T}/P_{u.T}$ values are given in Tables A1 to A7 and their variations with $\bar{\lambda}_{D.T}$ plots are depicted in Figs. 8(b) (*T=20*ºC) and 11 (*T≥100*ºC). The observation of the results presented in these figures lead to the following conclusions:

(i) Despite the inherent simplicity of the adjustments, the preliminary DSM distortional strength curves proposed provide fairly good ultimate load estimates for most of the ($i_1$) lipped channel and rack-section columns, and ($i_2$) three temperature-dependent steel constitutive models dealt with in this work. Indeed, the averages and standard deviations of the numerical $P^{*}_{n.D.T}/P_{u.T}$ values are comprised between ($i_1$) *0.90* (*T=100*ºC) and *0.97* (*T=300*, *500*ºC), and ($i_2$) *0.04* (*T=20*ºC) and *0.14* (*T=500*ºC).

(ii) The averages and standard deviations of the numerical $P_{n.D}/P_{u.T}$ values are clearly "wore": they vary between ($ii_1$) *1.04* (*T=20*ºC) and *1.19* (*T=400-600*ºC), and ($ii_2$) *0.07* (*T=20*ºC) and *0.13* (*T=300*ºC).

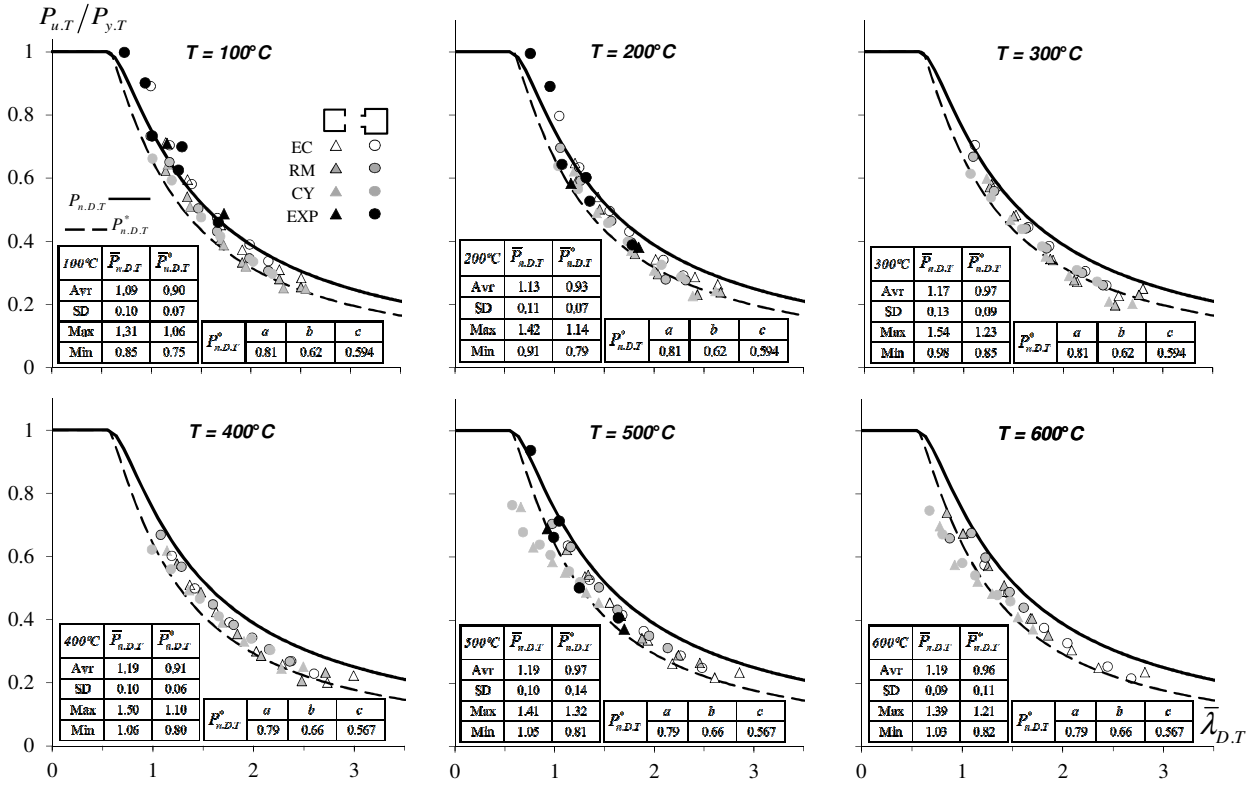


**Figure 10.** Comparison between the numerical/experimental column ultimate loads and proposed DSM estimates (*T≥100*ºC).

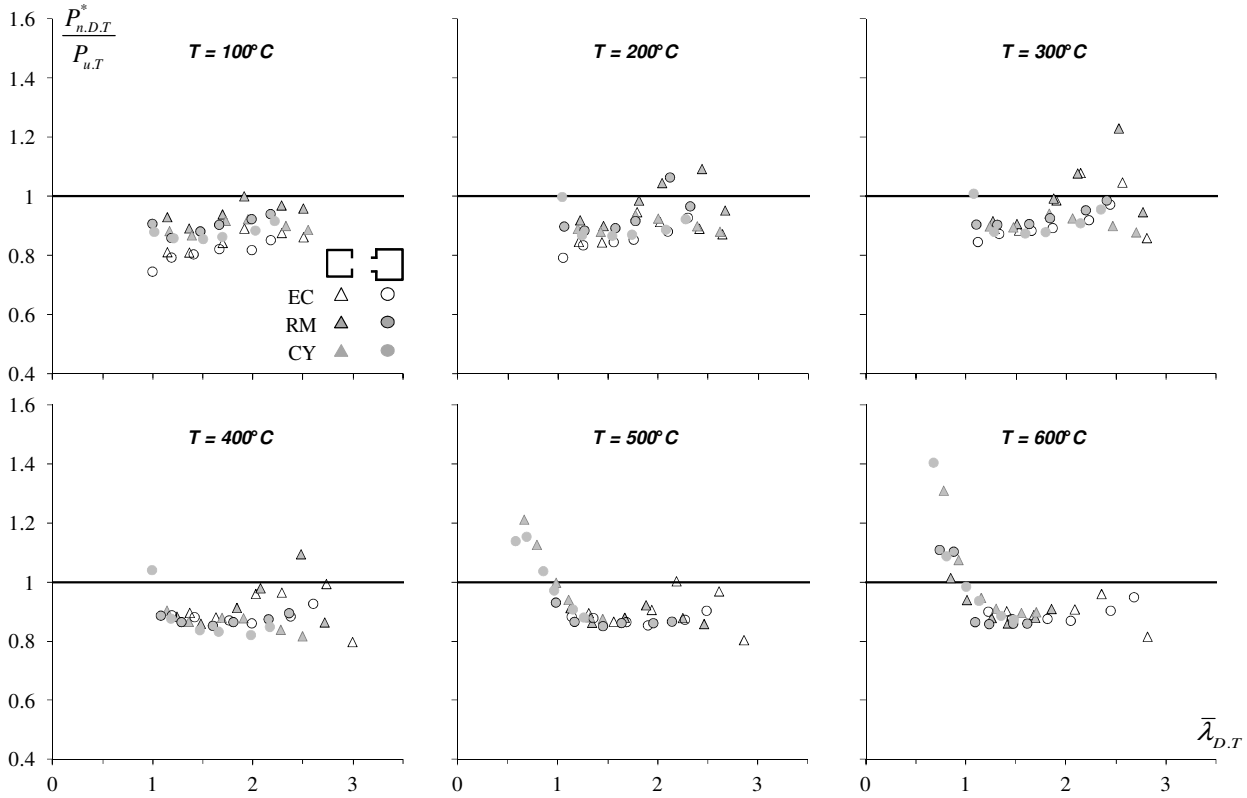


**Figure 11.** Varition of $P^*_{n.D.T}/P_{u.T}$ with $\bar{\lambda}_{D.T}$ for the six elevated temperatures.

(iii) Nevertheless, practically all the failure loads of the lipped channel and rack-section stocky columns analyzed with the CY model at *T=500-600*ºC are considerably overestimated by the proposed DSM distortional strength curves, *i.e.*, the corresponding ultimate load erosion is not adequately captured.

Finally, Fig. 12 compares (i) the proposed DSM distortional strength curves for elevated temperatures, given by Eq. (8) for the two temperature ranges *T=100-300*ºC and *T=400-600*ºC, and (ii) the current DSM design curve, given by Eq. (7) for *T=20*ºC. Note that the *T=100-300*ºC and *T=400-600*ºC curves practically coincide for $\bar{\lambda}_D \leq 1.00$, thus explaining why the latter is unable to capture the high ultimate strength erosion predicted by the CY (mostly) and RM models for this slenderness range at *T=500-600*ºC.

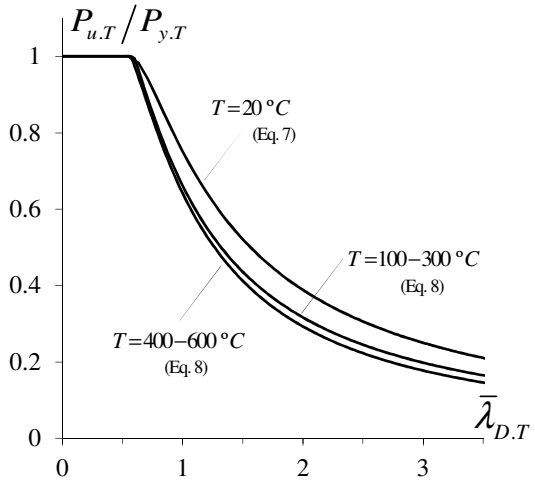


**Figure 12.** Comparison between the current (room temperature) and proposed (elevated temperatures) DSM distortional strength curves.

## 6. Conclusion

This paper reported a numerical (ANSYS SFEA) investigation aimed at assessing the performance of the current DSM distortional strength curve to estimate the failure loads of fixed-ended cold-formed steel lipped channel and rack-section columns (i) subjected to various uniform temperature distributions caused by fire conditions (up to *600*ºC), (ii) exhibiting several room-temperature yield stresses, selected to cover a wide distortional slenderness range, and (iii) displaying three different temperature-dependent steel stress-strain laws, namely the model prescribed in EC3-1.2 and the experimentally-based proposals of Chen & Young (2007a) and Ranawaka & Mahendran (2009a). The focus of the work was precisely to quantify the quality (accuracy and safety) of the current DSM distortional ultimate load predictions and to appraise how that quality was affected by the particular temperature-dependent steel constitutive model adopted. These goals were achieved by comparing the numerical distortional failure load data, obtained by means of non-linear SFEA incorporating small-amplitude critical-mode initial imperfections and involving *252* columns, with their current DSM estimates. The output of this comparison also led to the proposal of a few preliminary adjustments to improve the capture of the elevated temperature effects.

Out of the various findings unveiled in the course of this work, the following deserve a special mention:

(i) The $P_{u.T}/P_{y.T}$ *vs.* $\bar{\lambda}_{D.T}$ "clouds" concerning the numerical ultimate loads obtained with the three temperature-dependent steel constitutive model were shown to follow trends that can be accurately described by "Winter-type" strength/design curves (the few experimental distortional failure loads available in the literature also followed a similar trend). Moreover, the "vertical dispersion" was found to be perfectly acceptable for all of them, with one exception: the stocky columns subjected to $T=600$ ºC and analyzed with the model of Chen & Young (2007a).

(ii) The $P_{u.T}/P_{y.T}$ values of the columns at room temperature ($T=20$ºC) or subjected to $T=100$ºC were above those concerning the columns subjected to elevated temperatures ($T>100$ºC). This statement is also valid for the few experimental failure loads available.

(iii) The current DSM distortional ultimate strength estimates were found ($iii_1$) to be slightly (acceptably) unsafe for $\bar{\lambda}_D \leq 1.5$ and $T<400$ºC, ($iii_2$) to became progressively more unsafe as $\bar{\lambda}_D$ and/or $T$ increase and ($iii_3$) to be extremely unsafe for stocky columns analyzed with the Chen & Young (2007a) model at high temperatures, namely $T=500$ºC and $T=600$ºC.

(iv) A first attempt was made to find a unified DSM design approach to predict efficiently the numerical distortional failure loads of all the columns analyzed, regardless of the temperature value and/or steel constitutive model. It led to the incorporation of three (slightly) temperature-dependent parameters into the current DSM distortional strength expressions – different values for $T\leq 300$ºC and $T>300$ºC. In spite of the inherent simplicity of these adjustments, the ensuing DSM distortional strength curves were shown to provide fairly good ultimate load estimates for the vast majority of the columns.

(v) Indeed, the adjusted predicted-to-numerical ultimate load ratios averages and standard deviations are in the ranges *0.90-0.97* and *0.04-0.14* for all temperatures – the same intervals for their current DSM counterparts are *1.04-1.19* and *0.07-0.13*.

(vi) Finally, it seems fair to say that, on the basis of the limited amount of results reported in this work, an appropriate answer to the question appearing in the paper ("how relevant is the temperature dependence of the material behavior?") would be "not too much", as the conclusion drawn from this study apply more or less identically to the three temperature-dependent steel constitutive models considered.

To conclude, one last word to mention that the authors plan to extend the scope of this investigation to other (i) column geometries (cross-section shape/dimensions and length) and (ii) available temperature-

dependent constitutive models, namely those developed by Kankanamge & Mahendran (2011) and Wei & Jihong (2012). The corresponding results, which will be used to either confirm or supplement the findings obtained in this work, should be reported in the not too distant future.

## References


ABNT (2010). *Brazilian Standard on Design of Cold-Formed Steel Structures* (ABNT NBR 14762:2010), Brazilian Standards Association, Rio de Janeiro, RJ. (Portuguese)

AS/NZS (2005). *Cold-Formed Steel Structures*, Standards of Australia (SA) and Standards of New Zealand (SNZ), Sydney-Wellington.

Bebiano R, Pina P, Silvestre N, Camotim D (2008a). *GBTUL 1.0β – Buckling and Vibration Analysis of Thin-Walled Members*, DECivil/IST, Technical University of Lisbon. (http://www.civil.ist.utl.pt/gbt)

Bebiano R, Silvestre N, Camotim D (2008b). "GBTUL – A code for the buckling analysis of cold-formed steel members", *Proceedings of 19th International Specialty Conference on Recent Research and Developments in Cold-Formed Steel Design and Construction* (St. Louis, 14-15/10), R. LaBoube, W.W. Yu (eds.), 61-79.

BS5950-8 (1990). *Structural Use of Steelwork in Building – Part 8: Code of Practice for Fire Resistance Design*, British Standards Institution (BSI), London.

Chen J, Young B (2006). Corner properties of cold-formed steel sections at elevated temperatures, *Thin-Walled Structures*, **44**(2), 216-23.

Chen J, Young B (2007a). Experimental investigation of cold-formed steel material at elevated temperatures. *Thin-Walled Structures*, **45**(1), 96-110.

Chen J, Young B (2007b). Cold-formed steel lipped channel columns at elevated temperatures, *Engineering Structures*, **29**(10), 2445-56.

Chen J, Young B (2008). Design of high strength steel columns at elevated temperatures, *Journal of Constructional Steel Research*, **64**(6), 689-703.

EC3-1.2 (2005). *Eurocode 3: Design of Steel Structures – Part 1-2: General Rules – Structural Fire Design*, Comité Européen de Normalisation (CEN), Brussels.

Feng M, Wang YC (2005a). An analysis of the structural behaviour of axially loaded full-scale cold-formed thin-walled steel structural panels tested under fire conditions, *Thin-Walled Structures*, **43**(2), 291-332.

Feng M, Wang YC (2005b). An experimental study of loaded full-scale cold-formed thin-walled steel structural panels under fire conditions, *Fire Safety Journal*, **40**(1), 43-63.

Feng M, Wang YC, Davies JM (2003a). Structural behaviour of cold-formed thin-walled short steel channel columns at elevated temperatures – Part 1: experiments, *Thin-Walled Structures*, **41**(6), 543-70.

Feng M, Wang YC, Davies JM (2003b). Structural behaviour of cold-formed thin-walled short steel channel columns at elevated temperatures – Part 2: design calculations and numerical analysis, *Thin-Walled Structures*, **41**(6), 571-94.

Feng M, Wang YC, Davies JM (2003c). Thermal performance of cold-formed thin-walled steel panel systems in fire, *Fire Safety Journal*, **38**(4), 365-94.

Feng M, Wang YC, Davies JM (2003d). Axial strength of cold-formed thin-walled steel channels under non-uniform temperatures in fire, *Fire Safety Journal,* **38**(8), 679-707.

Feng M, Wang YC, Davies JM (2004). A numerical imperfection sensitivity study of cold-formed thin-walled tubular steel columns at uniform elevated temperatures, *Thin-Walled Structures*, **42**(4), 533-55.

Kaitila O (2002). Imperfection sensitivity analysis of lipped channel columns at high temperatures, *Journal of Constructional Steel Research*, **58**(3), 333-51.

Kankanamge ND, Mahendran M (2011). Mechanical properties of cold-formed steels at elevated temperatures, *Thin-Walled Structures*, **49**(1), 26-44.

Kirby BR, Preston RR (1988). High temperatures properties of hot-rolled structural steels for use in fire engineering design studies, *Fire Safety Journal*, **13**(1), 27-37.

Landesmann A, Camotim D (2010a). "Distortional failure and design of cold-formed steel lipped channel columns under fire conditions", *Proceedings of SSRC Annual Stability Conference* (Orlando, 12-15/5), 505-532.

Landesmann A, Camotim D (2010b). "Distortional failure and design of cold-formed steel rack-section columns under fire conditions", *Proceedings of Fourth International Conference on Steel & Composite Structures* (ICSCS'2011 – Sydney, 21-23/7), B. Uy *et al.* (eds.), 287-289. (full paper in CD-ROM Proceedings)

Landesmann A, Camotim D (2011). On the distortional buckling, post-buckling and strength of cold-formed steel lipped channel columns under fire conditions, *Journal of Structural Fire Engineering*, **2**(1), 1-19.

Landesmann A, Camotim D, Batista EM (2009). "On the distortional buckling, post-buckling and strength of cold-formed steel lipped channel columns subjected to elevated temperatures", *Proceedings of International Conference on Applications of Structural Fire Engineering* (Prague), F. Wald, P. Kallerová, J. Chlouba (eds.), A8-A13.

Lee JH, Mahendran M, Makelainen P (2003). Prediction of mechanical properties of light gauge steels at elevated temperatures, *Journal of Constructional Steel Research*, **59**(12), 1517-32.

Makelainen P, Outinen J, Kesti J (1998). Fire design model for structural steel S420M based upon transient-state tensile test results, *Journal of Constructional Steel Research*, **48**(1), 47-57.

Mecozzi E, Zhao B (2005). "Development of stress-strain relationships of cold-formed lightweight steel at elevated temperatures", *Proceedings of Fourth European Conference on Steel and Composite Structures* (EUROSTEEL'2005, Maastricht, 8-10/6) B. Hoffmeister, O. Hechler (eds.), 5.1/41-49 (vol. C).

Mirambell E, Real E (2000). On the calculation of deflections in structural stainless steel beams: an experimental and numerical investigation, *Journal of Constructional Steel Research,* **54**(1), 109-33.

NAS (2007). *North American Specification for the Design of Cold-Formed Steel Structural Members* (AISI-S100-07), American Iron and Steel Institute (AISI), Washington, DC.

Outinen J (1999). *Mechanical Properties of Structural Steels at Elevated Temperatures*, Licentiate Thesis, Helsinki University of Technology, Finland.

Outinen J, Kaitila O, Makelainen P (2000). "A study for the development of the design of steel structures in fire conditions", *Proceedings of First International Workshop on Structures in Fire* (SIF'2000 – Copenhagen, 19-20/6), J.M. Franssen (ed.), 267-281.

Outinen J, Kesti J, Makelainen P (1997). Fire design model for structural steel S355 based upon transient state tensile test results, *Journal of Constructional Steel Research*, **42**(3), 161-69.

Outinen J, Makelainen P. (2002). "Mechanical properties of structural steel at elevated temperatures, *Proceedings of Third International Conference on Advances in Steel Structures* (ICASS'2002 – Hong Kong, 9-11/12), S.L. Chan, J.G. Teng and K.F. Chung (eds.), 1103-1110.

Prola LC, Camotim D (2002a). "On the distortional post-buckling behavior of cold-formed lipped channel steel columns", *Proceedings of SSRC Annual Stability Conference* (Seattle, 24-27/4), 571-590.

Prola LC, Camotim D (2002b). "On the distortional post-buckling behaviour of rack-section cold-formed steel columns", *Proceedings of Sixth International Conference on Computational Structures Technology* (CST 2002 – Prague, 4-6/9), B. Topping, Z. Bittnar (eds.), Civil-Comp Press (Stirling), 233-234. (full paper in CD-ROM Proceedings – paper 98)

Ramberg W, Osgood WR (1943). *Description of stress–strain curves by three parameters*, NACA Technical Note 902.

Ranawaka T (2006). *Distortional Buckling Behaviour of Cold-Formed Steel Compression Members at Elevated Temperatures.* Ph.D. Thesis, Queensland University of Technology, Australia.

Ranawaka T, Mahendran M (2009a). Experimental study of the mechanical properties of light gauge cold-formed steels at elevated temperatures, *Fire Safety Journal*, **44**(2), 219–29.

Ranawaka T, Mahendran M (2009b). Distortional buckling tests of cold-formed steel compression members at elevated temperatures, *Journal of Constructional Steel Research*, **65**(2), 249-59.

Ranawaka T, Mahendran M (2010). Numerical modelling of light gauge cold-formed steel compression members subjected to distortional buckling at elevated temperatures, *Thin-Walled Structures*, **48**(3-4), 334-44.

Rasmussen KJR (2003). Full-range stress–strain curves for stainless steel alloys, *Journal of Constructional Steel Research*, **59**(1), 47-61.

SAS (Swanson Analysis Systems Inc.) (2009). *ANSYS Reference Manual* (version 12).

Schafer BW (2000). *Distortional Buckling of Cold-Formed Steel Columns*, American Iron and Steel Institute (AISI) Report, Washington DC.

Schafer BW (2005). *Direct Strength Method Design Guide*, American Iron and Steel Institute (AISI) Report, Washington DC.

Schafer BW (2008). Review: the Direct Strength Method of cold-formed steel member design, *Journal of Constructional Steel Research*, **64**(7-8), 766-88.

Schafer BW, Peköz T (1998). "Direct strength prediction of cold-formed steel members using numerical elastic buckling solutions", *Proceedings of 14th International Specialty Conference on Cold-formed Steel Structures* (St. Louis, 15-16/10), R. LaBoube, W.-W. Yu (eds.), 69-76.

Shahbazian A, Wang YC (2011a). Calculating the global buckling resistance of thin-walled steel members with uniform and non-uniform elevated temperatures under axial compression, *Thin-Walled Structures*, **49**(11), 1415-28.

Shahbazian A, Wang YC (2011b). Application of the Direct Strength Method to local buckling resistance of thin-walled steel members with non-uniform elevated temperatures under axial compression, *Thin-Walled Structures*, **49**(12), 1573-83.

Shahbazian A, Wang YC (2012). Direct Strength Method for calculating distortional buckling capacity of cold-formed thin-walled steel columns with uniform and non-uniform elevated temperatures, *Thin-Walled Structures*, **53**(Apr), 188-99.

Sidey MP, Teague DP (1988). *Elevated Temperature Data for Structural Grades of Galvanised Steel*. British Steel Report, Welsh Laboratories, UK.

Wei C, Jihong Y (2012). Mechanical properties of G550 cold-formed steel under transient and steady state conditions, *Journal of Constructional Steel Research*, in press. (doi.org/10.1016/j.jcsr.2011.12.010)

Zhao B, Kruppa J, Renaud C, O'Connor M, Mecozzi E *et al.* (2005), *Calculation Rules of Lightweight Steel Sections in Fire Situations*, EUR-21426 (Technical Steel Research Series) − Steel Products and Applications for Building, Construction and Industry, European Commission Technical Steel Research, Luxembourg.

## Annex

Tables A1 (room temperature) and A2-A7 (elevated temperatures) summarize the numerical (ANSYS SFEA) column ultimate strength and the corresponding DSM estimates obtained in the course of this investigation. Each table concerns both columns geometries (C130 and R135) and provides information about (i) the steel material model, including the corresponding $k_y$ and $k_e$ values for the temperatures considered, (ii) the critical (distortional) buckling loads $P_{cr}$, as well as the respective slenderness values $\bar{\lambda}_D$, (iii) the squash ($P_y$) and failure/ultimate ($P_u$) and loads, as well as the ratios between them ($P_u/P_y$), (iv) the ultimate strength estimates for the current ($P_{n.D}$) and modified ($P_{n.D}$) DSM strength curves, as well as the ratios $P_{n.D}/P_y$ and $P^*_{n.D}/P_y$, and (v) the current ($P_{n.D}/P_y$) and modified ($P^*_{n.D}/P_y$) predicted-to-numerical ultimate load ratios.

Table A1: Numerical ultimate loads and DSM estimates concerning the columns analyzed at *20* ºC.

| *Column* | $\sigma$-$\varepsilon$ | $k_y$ | $k_E$ | $P_{cr}$ (*kN*) | $\bar{\lambda}_D$ | $P_y$ (*kN*) | $P_u$ (*kN*) | $P_{n.D}$ (*kN*) | $\frac{P_u}{P_y}$ | $\frac{P_{n.D}}{P_y}$ | $\frac{P_{n.D}}{P_u}$ | $P^*_{n.D}$ (*kN*) | $\frac{P^*_{n.D}}{P_y}$ | $\frac{P^*_{n.D}}{P_u}$ |
|---|---|---|---|---|---|---|---|---|---|---|---|---|---|---|
| C130 | EC | 1.000 | 1.000 | 135.97 | 1.14 | 177.5 | 126.5 | 119.0 | 0.71 | 0.67 | 0.94 | 102.7 | 0.58 | 0.81 |
| | | | | | 1.36 | 252.1 | 150.0 | 144.0 | 0.60 | 0.57 | 0.96 | 121.7 | 0.48 | 0.81 |
| | | | | | 1.69 | 390.5 | 176.1 | 179.8 | 0.45 | 0.46 | 1.02 | 148.6 | 0.38 | 0.84 |
| | | | | | 1.91 | 497.0 | 185.3 | 202.1 | 0.37 | 0.41 | 1.09 | 165.3 | 0.33 | 0.89 |
| | | | | | 2.29 | 710.0 | 219.7 | 238.9 | 0.31 | 0.34 | 1.09 | 192.7 | 0.27 | 0.88 |
| | | | | | 2.50 | 852.0 | 241.1 | 259.7 | 0.28 | 0.30 | 1.08 | 208.1 | 0.24 | 0.86 |
| | RM | 1.000 | 1.000 | 135.97 | 1.14 | 177.5 | 124.4 | 119.0 | 0.70 | 0.67 | 0.96 | 102.7 | 0.58 | 0.83 |
| | | | | | 1.36 | 252.1 | 154.0 | 144.0 | 0.61 | 0.57 | 0.94 | 121.7 | 0.48 | 0.79 |
| | | | | | 1.69 | 390.5 | 176.3 | 179.8 | 0.45 | 0.46 | 1.02 | 148.6 | 0.38 | 0.84 |
| | | | | | 1.91 | 497.0 | 185.4 | 202.1 | 0.37 | 0.41 | 1.09 | 165.3 | 0.33 | 0.89 |
| | | | | | 2.29 | 710.0 | 215.6 | 238.9 | 0.30 | 0.34 | 1.11 | 192.7 | 0.27 | 0.89 |
| | | | | | 2.50 | 852.0 | 233.2 | 259.7 | 0.27 | 0.30 | 1.11 | 208.1 | 0.24 | 0.89 |
| | CY | 1.000 | 1.000 | 135.97 | 1.14 | 177.5 | 117.9 | 119.0 | 0.66 | 0.67 | 1.01 | 102.7 | 0.58 | 0.87 |
| | | | | | 1.36 | 252.1 | 142.1 | 144.0 | 0.56 | 0.57 | 1.01 | 121.7 | 0.48 | 0.86 |
| | | | | | 1.69 | 390.5 | 162.9 | 179.8 | 0.42 | 0.46 | 1.10 | 148.6 | 0.38 | 0.91 |
| | | | | | 1.91 | 497.0 | 179.5 | 202.1 | 0.36 | 0.41 | 1.13 | 165.3 | 0.33 | 0.92 |
| | | | | | 2.29 | 710.0 | 213.5 | 238.9 | 0.30 | 0.34 | 1.12 | 192.7 | 0.27 | 0.90 |
| | | | | | 2.50 | 852.0 | 234.0 | 259.7 | 0.27 | 0.30 | 1.11 | 208.1 | 0.24 | 0.89 |
| R135 | EC | 1.000 | 1.000 | 256.21 | 0.99 | 252.5 | 224.8 | 190.5 | 0.89 | 0.75 | 0.85 | 167.8 | 0.66 | 0.75 |
| | | | | | 1.18 | 358.6 | 252.3 | 233.2 | 0.70 | 0.65 | 0.92 | 200.3 | 0.56 | 0.79 |
| | | | | | 1.40 | 505.0 | 293.1 | 280.2 | 0.58 | 0.55 | 0.96 | 235.9 | 0.47 | 0.80 |
| | | | | | 1.66 | 707.0 | 334.3 | 332.2 | 0.47 | 0.47 | 0.99 | 275.1 | 0.39 | 0.82 |
| | | | | | 1.99 | 1010.0 | 392.8 | 394.8 | 0.39 | 0.39 | 1.01 | 321.9 | 0.32 | 0.82 |
| | | | | | 2.17 | 1212.0 | 408.0 | 430.1 | 0.34 | 0.35 | 1.05 | 348.1 | 0.29 | 0.85 |
| | RM | 1.000 | 1.000 | 256.21 | 0.99 | 252.5 | 184.5 | 190.5 | 0.73 | 0.75 | 1.03 | 167.8 | 0.66 | 0.91 |
| | | | | | 1.18 | 358.6 | 232.6 | 233.2 | 0.65 | 0.65 | 1.00 | 200.3 | 0.56 | 0.86 |
| | | | | | 1.47 | 555.5 | 279.1 | 294.3 | 0.50 | 0.53 | 1.05 | 246.6 | 0.44 | 0.88 |
| | | | | | 1.66 | 707.0 | 303.6 | 332.2 | 0.43 | 0.47 | 1.09 | 275.1 | 0.39 | 0.91 |
| | | | | | 1.99 | 1010.0 | 347.9 | 394.8 | 0.34 | 0.39 | 1.13 | 321.9 | 0.32 | 0.93 |
| | | | | | 2.17 | 1212.0 | 390.0 | 430.1 | 0.32 | 0.35 | 1.10 | 348.1 | 0.29 | 0.89 |
| | CY | 1.000 | 1.000 | 256.21 | 0.99 | 252.5 | 194.1 | 190.5 | 0.77 | 0.75 | 0.98 | 167.8 | 0.66 | 0.86 |
| | | | | | 1.18 | 358.6 | 238.1 | 233.2 | 0.66 | 0.65 | 0.98 | 200.3 | 0.56 | 0.84 |
| | | | | | 1.47 | 555.5 | 291.6 | 294.3 | 0.52 | 0.53 | 1.01 | 246.6 | 0.44 | 0.85 |
| | | | | | 1.66 | 707.0 | 321.2 | 332.2 | 0.45 | 0.47 | 1.03 | 275.1 | 0.39 | 0.86 |
| | | | | | 1.99 | 1010.0 | 367.0 | 394.8 | 0.36 | 0.39 | 1.08 | 321.9 | 0.32 | 0.88 |
| | | | | | 2.17 | 1212.0 | 384.9 | 430.1 | 0.32 | 0.35 | 1.12 | 348.1 | 0.29 | 0.90 |

Note: EC (EC3-1.2 2005), CY (Chen & Young 2007a) and RM (Ranawaka & Mahendran 2009a)

Table A2: Numerical ultimate loads and DSM estimates concerning the columns analyzed at *100* ºC.

| *Column* | $\sigma$-$\varepsilon$ | $k_y$ | $k_E$ | $P_{cr}$ ($kN$) | $\bar{\lambda}_D$ | $P_y$ ($kN$) | $P_u$ ($kN$) | $P_{n.D}$ ($kN$) | $\frac{P_u}{P_y}$ | $\frac{P_{n.D}}{P_y}$ | $\frac{P_{n.D}}{P_u}$ | $P^*_{n.D}$ ($kN$) | $\frac{P^*_{n.D}}{P_y}$ | $\frac{P^*_{n.D}}{P_u}$ |
|---|---|---|---|---|---|---|---|---|---|---|---|---|---|---|
| C130 | EC | 1.000 | 1.000 | 135.97 | 1.14 | 177.5 | 126.5 | 119.0 | 0.71 | 0.67 | 0.94 | 102.7 | 0.58 | 0.81 |
| | | | | | 1.36 | 252.1 | 150.0 | 144.0 | 0.60 | 0.57 | 0.96 | 121.7 | 0.48 | 0.81 |
| | | | | | 1.69 | 390.5 | 176.1 | 179.8 | 0.45 | 0.46 | 1.02 | 148.6 | 0.38 | 0.84 |
| | | | | | 1.91 | 497.0 | 185.3 | 202.1 | 0.37 | 0.41 | 1.09 | 165.3 | 0.33 | 0.89 |
| | | | | | 2.29 | 710.0 | 219.7 | 238.9 | 0.31 | 0.34 | 1.09 | 192.7 | 0.27 | 0.88 |
| | | | | | 2.50 | 852.0 | 241.1 | 259.7 | 0.28 | 0.30 | 1.08 | 208.1 | 0.24 | 0.86 |
| | RM | 0.998 | 1.000 | 135.97 | 1.14 | 177.1 | 110.3 | 118.9 | 0.67 | 1.08 | 1.08 | 102.6 | 0.58 | 0.93 |
| | | | | | 1.36 | 251.5 | 136.1 | 143.8 | 0.57 | 1.06 | 1.06 | 121.5 | 0.48 | 0.89 |
| | | | | | 1.69 | 389.7 | 157.9 | 179.7 | 0.46 | 1.14 | 1.14 | 148.5 | 0.38 | 0.94 |
| | | | | | 1.91 | 496.0 | 164.9 | 201.9 | 0.41 | 1.22 | 1.22 | 165.1 | 0.33 | 1.00 |
| | | | | | 2.28 | 708.6 | 198.4 | 238.7 | 0.34 | 1.20 | 1.20 | 192.5 | 0.27 | 0.97 |
| | | | | | 2.50 | 850.3 | 216.5 | 259.5 | 0.31 | 1.20 | 1.20 | 207.9 | 0.24 | 0.96 |
| | CY | 0.972 | 0.938 | 127.54 | 1.16 | 172.5 | 111.0 | 113.9 | 0.66 | 1.03 | 1.03 | 98.1 | 0.57 | 0.88 |
| | | | | | 1.39 | 245.0 | 124.7 | 137.6 | 0.56 | 1.10 | 1.10 | 116.0 | 0.47 | 0.93 |
| | | | | | 1.73 | 379.6 | 147.0 | 171.7 | 0.45 | 1.17 | 1.17 | 141.6 | 0.37 | 0.96 |
| | | | | | 1.95 | 483.1 | 154.7 | 192.8 | 0.40 | 1.25 | 1.25 | 157.5 | 0.33 | 1.02 |
| | | | | | 2.33 | 690.1 | 173.3 | 227.8 | 0.33 | 1.31 | 1.31 | 183.5 | 0.27 | 1.06 |
| | | | | | 2.55 | 828.1 | 206.6 | 247.6 | 0.30 | 1.20 | 1.20 | 198.1 | 0.24 | 0.96 |
| R135 | EC | 1.000 | 1.000 | 256.21 | 0.99 | 252.5 | 224.8 | 190.5 | 0.75 | 0.85 | 0.85 | 167.8 | 0.66 | 0.75 |
| | | | | | 1.18 | 358.6 | 252.3 | 233.2 | 0.65 | 0.92 | 0.92 | 200.3 | 0.56 | 0.79 |
| | | | | | 1.40 | 505.0 | 293.1 | 280.2 | 0.55 | 0.96 | 0.96 | 235.9 | 0.47 | 0.80 |
| | | | | | 1.66 | 707.0 | 334.3 | 332.2 | 0.47 | 0.99 | 0.99 | 275.1 | 0.39 | 0.82 |
| | | | | | 1.99 | 1010.0 | 392.8 | 394.8 | 0.39 | 1.01 | 1.01 | 321.9 | 0.32 | 0.82 |
| | | | | | 2.17 | 1212.0 | 408.0 | 430.1 | 0.35 | 1.05 | 1.05 | 348.1 | 0.29 | 0.85 |
| | RM | 0.998 | 1.000 | 256.21 | 0.99 | 252.0 | 184.5 | 190.3 | 0.75 | 1.03 | 1.03 | 167.6 | 0.67 | 0.91 |
| | | | | | 1.18 | 357.8 | 232.6 | 232.9 | 0.65 | 1.00 | 1.00 | 200.2 | 0.56 | 0.86 |
| | | | | | 1.47 | 554.4 | 279.1 | 294.0 | 0.53 | 1.05 | 1.05 | 246.3 | 0.44 | 0.88 |
| | | | | | 1.66 | 705.6 | 303.6 | 331.9 | 0.47 | 1.09 | 1.09 | 274.8 | 0.39 | 0.91 |
| | | | | | 1.98 | 1008.0 | 347.9 | 394.4 | 0.39 | 1.13 | 1.13 | 321.6 | 0.32 | 0.92 |
| | | | | | 2.17 | 1209.6 | 369.5 | 429.7 | 0.36 | 1.16 | 1.16 | 347.8 | 0.29 | 0.94 |
| | CY | 0.972 | 0.938 | 240.32 | 1.01 | 245.4 | 162.3 | 182.5 | 0.74 | 1.12 | 1.12 | 160.4 | 0.65 | 0.99 |
| | | | | | 1.20 | 348.5 | 206.4 | 223.1 | 0.64 | 1.08 | 1.08 | 191.2 | 0.55 | 0.93 |
| | | | | | 1.50 | 539.9 | 256.8 | 281.1 | 0.52 | 1.09 | 1.09 | 235.1 | 0.44 | 0.92 |
| | | | | | 1.69 | 687.2 | 285.1 | 317.2 | 0.46 | 1.11 | 1.11 | 262.2 | 0.38 | 0.92 |
| | | | | | 2.02 | 981.7 | 328.7 | 376.6 | 0.38 | 1.15 | 1.15 | 306.6 | 0.31 | 0.93 |
| | | | | | 2.21 | 1178.1 | 349.2 | 410.2 | 0.35 | 1.17 | 1.17 | 331.5 | 0.28 | 0.95 |

Table A3: Numerical ultimate loads and DSM estimates concerning the columns analyzed at *200* ºC.

| *Column* | $\sigma$-$\varepsilon$ | $k_y$ | $k_E$ | $P_{cr}$ ($kN$) | $\bar{\lambda}_D$ | $P_y$ ($kN$) | $P_u$ ($kN$) | $P_{n.D}$ ($kN$) | $\frac{P_u}{P_y}$ | $\frac{P_{n.D}}{P_y}$ | $\frac{P_{n.D}}{P_u}$ | $P^*_{n.D}$ ($kN$) | $\frac{P^*_{n.D}}{P_y}$ | $\frac{P^*_{n.D}}{P_u}$ |
|---|---|---|---|---|---|---|---|---|---|---|---|---|---|---|
| C130 | EC | 1.000 | 0.900 | 122.37 | 1.20 | 177.5 | 114.9 | 113.6 | 0.65 | 0.64 | 0.99 | 97.4 | 0.55 | 0.85 |
| | | | | | 1.44 | 252.1 | 136.0 | 136.9 | 0.54 | 0.54 | 1.01 | 115.0 | 0.46 | 0.85 |
| | | | | | 1.79 | 390.5 | 147.9 | 170.4 | 0.38 | 0.44 | 1.15 | 140.2 | 0.36 | 0.95 |
| | | | | | 2.02 | 497.0 | 170.3 | 191.3 | 0.34 | 0.38 | 1.12 | 155.7 | 0.31 | 0.91 |
| | | | | | 2.41 | 710.0 | 203.4 | 225.7 | 0.29 | 0.32 | 1.11 | 181.3 | 0.26 | 0.89 |
| | | | | | 2.64 | 852.0 | 224.1 | 245.2 | 0.26 | 0.29 | 1.09 | 195.7 | 0.23 | 0.87 |
| | RM | 0.987 | 0.870 | 118.29 | 1.22 | 175.2 | 103.4 | 111.1 | 0.63 | 1.07 | 1.07 | 95.1 | 0.54 | 0.92 |
| | | | | | 1.45 | 248.8 | 124.6 | 133.8 | 0.54 | 1.07 | 1.07 | 112.2 | 0.45 | 0.90 |
| | | | | | 1.81 | 385.4 | 138.5 | 166.4 | 0.43 | 1.20 | 1.20 | 136.7 | 0.35 | 0.99 |
| | | | | | 2.04 | 490.5 | 145.2 | 186.7 | -0.38 | 1.29 | 1.29 | 151.9 | 0.31 | 1.05 |
| | | | | | 2.43 | 700.8 | 161.6 | 220.3 | -0.31 | 1.36 | 1.36 | 176.8 | 0.25 | 1.09 |
| | | | | | 2.67 | 840.9 | 200.1 | 239.2 | -0.28 | 1.20 | 1.20 | 190.8 | 0.23 | 0.95 |
| | CY | 0.936 | 0.858 | 116.66 | 1.19 | 166.1 | 103.3 | 107.2 | 0.65 | 1.04 | 1.04 | 92.0 | 0.55 | 0.89 |
| | | | | | 1.42 | 235.9 | 115.3 | 129.3 | 0.55 | 1.12 | 1.12 | 108.7 | 0.46 | 0.94 |
| | | | | | 1.77 | 365.5 | 135.1 | 161.0 | 0.44 | 1.19 | 1.19 | 132.5 | 0.36 | 0.98 |
| | | | | | 2.00 | 465.2 | 142.8 | 180.7 | -0.39 | 1.27 | 1.27 | 147.3 | 0.32 | 1.03 |
| | | | | | 2.39 | 664.6 | 150.5 | 213.4 | -0.32 | 1.42 | 1.42 | 171.5 | 0.26 | 1.14 |
| | | | | | 2.61 | 797.5 | 193.3 | 231.8 | -0.29 | 1.20 | 1.20 | 185.1 | 0.23 | 0.96 |
| R135 | EC | 1.000 | 0.900 | 230.59 | 1.05 | 252.5 | 201.0 | 182.5 | 0.72 | 0.91 | 0.91 | 159.5 | 0.63 | 0.79 |
| | | | | | 1.25 | 358.6 | 227.2 | 222.3 | 0.62 | 0.98 | 0.98 | 189.8 | 0.53 | 0.84 |
| | | | | | 1.55 | 555.5 | 275.1 | 279.4 | 0.50 | 1.02 | 1.02 | 232.9 | 0.42 | 0.85 |
| | | | | | 1.75 | 707.0 | 303.6 | 314.9 | 0.45 | 1.04 | 1.04 | 259.5 | 0.37 | 0.85 |
| | | | | | 2.09 | 1010.0 | 343.6 | 373.4 | 0.37 | 1.09 | 1.09 | 303.1 | 0.30 | 0.88 |
| | | | | | 2.29 | 1212.0 | 352.8 | 406.5 | 0.34 | 1.15 | 1.15 | 327.7 | 0.27 | 0.93 |
| | RM | 0.987 | 0.870 | 222.90 | 1.06 | 249.2 | 173.3 | 178.6 | 0.72 | 1.03 | 1.03 | 155.8 | 0.63 | 0.90 |
| | | | | | 1.26 | 353.9 | 209.3 | 217.4 | 0.61 | 1.04 | 1.04 | 185.3 | 0.52 | 0.89 |
| | | | | | 1.57 | 548.3 | 254.3 | 273.0 | 0.50 | 1.07 | 1.07 | 227.2 | 0.41 | 0.89 |
| | | | | | 1.77 | 697.8 | 275.8 | 307.5 | 0.44 | 1.11 | 1.11 | 253.1 | 0.36 | 0.92 |
| | | | | | 2.11 | 996.9 | 277.5 | 364.5 | 0.37 | 1.31 | 1.31 | 295.7 | 0.30 | 1.07 |
| | | | | | 2.32 | 1196.2 | 330.3 | 396.7 | 0.33 | 1.20 | 1.20 | 319.6 | 0.27 | 0.97 |
| | CY | 0.936 | 0.858 | 219.83 | 1.04 | 236.3 | 150.7 | 172.1 | 0.73 | 1.14 | 1.14 | 150.6 | 0.64 | 1.00 |
| | | | | | 1.24 | 335.6 | 189.6 | 209.9 | 0.63 | 1.11 | 1.11 | 179.3 | 0.53 | 0.95 |
| | | | | | 1.54 | 519.9 | 237.7 | 263.9 | 0.51 | 1.11 | 1.11 | 220.1 | 0.42 | 0.93 |
| | | | | | 1.74 | 661.8 | 263.5 | 297.5 | 0.45 | 1.13 | 1.13 | 245.4 | 0.37 | 0.93 |
| | | | | | 2.07 | 945.4 | 307.1 | 352.9 | 0.37 | 1.15 | 1.15 | 286.7 | 0.30 | 0.93 |
| | | | | | 2.27 | 1134.4 | 325.3 | 384.2 | 0.34 | 1.18 | 1.18 | 310.0 | 0.27 | 0.95 |

Table A4: Numerical ultimate loads and DSM estimates concerning the columns analyzed at *300* ºC.

| *Column* | $\sigma$-$\varepsilon$ | $k_y$ | $k_E$ | $P_{cr}$ ($kN$) | $\bar{\lambda}_D$ | $P_y$ ($kN$) | $P_u$ ($kN$) | $P_{n.D}$ ($kN$) | $\frac{P_u}{P_y}$ | $\frac{P_{n.D}}{P_y}$ | $\frac{P_{n.D}}{P_u}$ | $P^*_{n.D}$ ($kN$) | $\frac{P^*_{n.D}}{P_y}$ | $\frac{P^*_{n.D}}{P_u}$ |
|---|---|---|---|---|---|---|---|---|---|---|---|---|---|---|
| C130 | EC | 1.000 | 0.800 | 108.78 | 1.28 | 177.5 | 102.9 | 107.7 | 0.58 | 0.61 | 1.05 | 91.6 | 0.52 | 0.89 |
| | | | | | 1.52 | 252.1 | 121.9 | 129.2 | 0.48 | 0.51 | 1.06 | 107.9 | 0.43 | 0.89 |
| | | | | | 1.89 | 390.5 | 132.8 | 160.3 | 0.34 | 0.41 | 1.21 | 131.2 | 0.34 | 0.99 |
| | | | | | 2.14 | 497.0 | 134.8 | 179.7 | 0.27 | 0.36 | 1.33 | 145.6 | 0.29 | 1.08 |
| | | | | | 2.55 | 710.0 | 161.6 | 211.7 | 0.23 | 0.30 | 1.31 | 169.3 | 0.24 | 1.05 |
| | | | | | 2.80 | 852.0 | 212.4 | 229.8 | 0.25 | 0.27 | 1.08 | 182.7 | 0.21 | 0.86 |
| | RM | 0.899 | 0.740 | 100.62 | 1.26 | 159.6 | 91.1 | 98.1 | 0.61 | 1.08 | 1.08 | 83.6 | 0.52 | 0.92 |
| | | | | | 1.50 | 226.6 | 108.5 | 117.8 | 0.52 | 1.09 | 1.09 | 98.5 | 0.43 | 0.91 |
| | | | | | 1.87 | 351.1 | 120.6 | 146.3 | 0.42 | 1.21 | 1.21 | 119.9 | 0.34 | 0.99 |
| | | | | | 2.11 | 446.8 | 123.3 | 164.0 | 0.37 | 1.33 | 1.33 | 133.1 | 0.30 | 1.08 |
| | | | | | 2.52 | 638.3 | 125.7 | 193.3 | 0.30 | 1.54 | 1.54 | 154.8 | 0.24 | 1.23 |
| | | | | | 2.76 | 765.9 | 176.2 | 209.9 | 0.27 | 1.19 | 1.19 | 167.0 | 0.22 | 0.95 |
| | CY | 0.900 | 0.778 | 105.78 | 1.23 | 159.8 | 95.4 | 100.4 | 0.63 | 1.05 | 1.05 | 85.8 | 0.54 | 0.90 |
| | | | | | 1.46 | 226.8 | 106.0 | 120.8 | 0.53 | 1.14 | 1.14 | 101.3 | 0.45 | 0.96 |
| | | | | | 1.82 | 351.5 | 123.4 | 150.2 | 0.43 | 1.22 | 1.22 | 123.3 | 0.35 | 1.00 |
| | | | | | 2.06 | 447.3 | 129.7 | 168.5 | 0.38 | 1.30 | 1.30 | 137.0 | 0.31 | 1.06 |
| | | | | | 2.46 | 639.0 | 133.0 | 198.7 | 0.31 | 1.49 | 1.49 | 159.4 | 0.25 | 1.20 |
| | | | | | 2.69 | 766.8 | 154.4 | 215.8 | 0.28 | 1.40 | 1.40 | 172.0 | 0.22 | 1.11 |
| R135 | EC | 1.000 | 0.800 | 204.97 | 1.11 | 252.5 | 177.7 | 173.7 | 0.69 | 0.98 | 0.98 | 150.5 | 0.60 | 0.85 |
| | | | | | 1.32 | 358.6 | 204.1 | 210.5 | 0.59 | 1.03 | 1.03 | 178.4 | 0.50 | 0.87 |
| | | | | | 1.65 | 555.5 | 246.7 | 263.4 | 0.47 | 1.07 | 1.07 | 218.3 | 0.39 | 0.88 |
| | | | | | 1.86 | 707.0 | 271.8 | 296.3 | 0.42 | 1.09 | 1.09 | 242.9 | 0.34 | 0.89 |
| | | | | | 2.22 | 1010.0 | 307.8 | 350.7 | 0.35 | 1.14 | 1.14 | 283.4 | 0.28 | 0.92 |
| | | | | | 2.43 | 1212.0 | 314.5 | 381.4 | 0.31 | 1.21 | 1.21 | 306.1 | 0.25 | 0.97 |
| | RM | 0.899 | 0.740 | 189.60 | 1.09 | 227.0 | 151.5 | 158.0 | 0.70 | 1.04 | 1.04 | 137.2 | 0.60 | 0.91 |
| | | | | | 1.30 | 322.3 | 179.9 | 191.8 | 0.60 | 1.07 | 1.07 | 162.8 | 0.51 | 0.91 |
| | | | | | 1.62 | 499.4 | 219.7 | 240.2 | 0.48 | 1.09 | 1.09 | 199.4 | 0.40 | 0.91 |
| | | | | | 1.83 | 635.6 | 239.3 | 270.4 | 0.43 | 1.13 | 1.13 | 221.9 | 0.35 | 0.93 |
| | | | | | 2.19 | 908.0 | 271.4 | 320.1 | 0.35 | 1.18 | 1.18 | 259.0 | 0.29 | 0.95 |
| | | | | | 2.40 | 1089.6 | 283.4 | 348.2 | 0.32 | 1.23 | 1.23 | 279.8 | 0.26 | 0.99 |
| | CY | 0.900 | 0.778 | 199.33 | 1.07 | 227.3 | 139.3 | 161.5 | 0.71 | 1.16 | 1.16 | 140.7 | 0.62 | 1.01 |
| | | | | | 1.27 | 322.7 | 173.6 | 196.4 | 0.61 | 1.13 | 1.13 | 167.3 | 0.52 | 0.96 |
| | | | | | 1.58 | 500.0 | 219.0 | 246.5 | 0.49 | 1.13 | 1.13 | 205.0 | 0.41 | 0.94 |
| | | | | | 1.79 | 636.3 | 243.6 | 277.6 | 0.44 | 1.14 | 1.14 | 228.3 | 0.36 | 0.94 |
| | | | | | 2.14 | 909.0 | 280.3 | 328.9 | 0.36 | 1.17 | 1.17 | 266.6 | 0.29 | 0.95 |
| | | | | | 2.34 | 1090.8 | 296.2 | 357.9 | 0.33 | 1.21 | 1.21 | 288.1 | 0.26 | 0.97 |

Table A5: Numerical ultimate loads and DSM estimates concerning the columns analyzed at *400* ºC.

| *Column* | $\sigma$-$\varepsilon$ | $k_y$ | $k_E$ | $P_{cr}$ ($kN$) | $\bar{\lambda}_D$ | $P_y$ ($kN$) | $P_u$ ($kN$) | $P_{n.D}$ ($kN$) | $\frac{P_u}{P_y}$ | $\frac{P_{n.D}}{P_y}$ | $\frac{P_{n.D}}{P_u}$ | $P^*_{n.D}$ ($kN$) | $\frac{P^*_{n.D}}{P_y}$ | $\frac{P^*_{n.D}}{P_u}$ |
|---|---|---|---|---|---|---|---|---|---|---|---|---|---|---|
| C130 | EC | 1.000 | 0.700 | 95.18 | 1.37 | 177.5 | 90.5 | 101.1 | 0.51 | 0.57 | 1.12 | 81.2 | 0.46 | 0.90 |
| | | | | | 1.63 | 252.1 | 106.8 | 120.9 | 0.42 | 0.48 | 1.13 | 94.3 | 0.37 | 0.88 |
| | | | | | 2.03 | 390.5 | 116.8 | 149.5 | 0.30 | 0.38 | 1.28 | 112.4 | 0.29 | 0.96 |
| | | | | | 2.29 | 497.0 | 127.7 | 167.3 | 0.26 | 0.34 | 1.31 | 123.5 | 0.25 | 0.97 |
| | | | | | 2.73 | 710.0 | 142.0 | 196.7 | 0.20 | 0.28 | 1.39 | 141.4 | 0.20 | 1.00 |
| | | | | | 2.99 | 852.0 | 189.4 | 213.4 | 0.22 | 0.25 | 1.13 | 151.3 | 0.18 | 0.80 |
| | RM | 0.717 | 0.610 | 82.94 | 1.24 | 127.3 | 73.3 | 79.4 | 0.62 | 1.08 | 1.08 | 64.9 | 0.51 | 0.89 |
| | | | | | 1.48 | 180.7 | 87.8 | 95.5 | 0.53 | 1.09 | 1.09 | 75.7 | 0.42 | 0.86 |
| | | | | | 1.84 | 280.0 | 99.1 | 118.7 | 0.42 | 1.20 | 1.20 | 90.7 | 0.32 | 0.92 |
| | | | | | 2.07 | 356.3 | 101.6 | 133.1 | 0.37 | 1.31 | 1.31 | 99.8 | 0.28 | 0.98 |
| | | | | | 2.48 | 509.1 | 104.4 | 157.0 | 0.31 | 1.50 | 1.50 | 114.5 | 0.22 | 1.10 |
| | | | | | 2.71 | 610.9 | 141.7 | 170.4 | 0.28 | 1.20 | 1.20 | 122.6 | 0.20 | 0.87 |
| | CY | 0.692 | 0.698 | 94.91 | 1.14 | 122.8 | 75.9 | 82.7 | 0.67 | 1.09 | 1.09 | 68.7 | 0.56 | 0.91 |
| | | | | | 1.36 | 174.4 | 86.0 | 100.1 | 0.57 | 1.16 | 1.16 | 80.5 | 0.46 | 0.94 |
| | | | | | 1.69 | 270.2 | 105.3 | 125.0 | 0.46 | 1.19 | 1.19 | 96.8 | 0.36 | 0.92 |
| | | | | | 1.90 | 343.9 | 113.5 | 140.5 | 0.41 | 1.24 | 1.24 | 106.7 | 0.31 | 0.94 |
| | | | | | 2.28 | 491.3 | 120.1 | 166.1 | 0.34 | 1.38 | 1.38 | 122.7 | 0.25 | 1.02 |
| | | | | | 2.49 | 589.6 | 147.8 | 180.6 | 0.31 | 1.22 | 1.22 | 131.6 | 0.22 | 0.89 |
| R135 | EC | 1.000 | 0.700 | 179.35 | 1.19 | 252.5 | 151.7 | 163.8 | 0.65 | 1.08 | 1.08 | 135.0 | 0.53 | 0.89 |
| | | | | | 1.41 | 358.6 | 178.5 | 197.6 | 0.55 | 1.11 | 1.11 | 157.8 | 0.44 | 0.88 |
| | | | | | 1.76 | 555.5 | 217.0 | 246.1 | 0.44 | 1.13 | 1.13 | 189.4 | 0.34 | 0.87 |
| | | | | | 1.99 | 707.0 | 241.7 | 276.4 | 0.39 | 1.14 | 1.14 | 208.5 | 0.29 | 0.86 |
| | | | | | 2.37 | 1010.0 | 270.3 | 326.3 | 0.32 | 1.21 | 1.21 | 239.5 | 0.24 | 0.89 |
| | | | | | 2.60 | 1212.0 | 276.3 | 354.5 | 0.29 | 1.28 | 1.28 | 256.7 | 0.21 | 0.93 |
| | RM | 0.717 | 0.610 | 156.29 | 1.08 | 181.0 | 120.9 | 127.8 | 0.71 | 1.06 | 1.06 | 107.4 | 0.59 | 0.89 |
| | | | | | 1.28 | 257.1 | 145.6 | 155.3 | 0.60 | 1.07 | 1.07 | 126.2 | 0.49 | 0.87 |
| | | | | | 1.60 | 398.3 | 178.3 | 194.8 | 0.49 | 1.09 | 1.09 | 152.3 | 0.38 | 0.85 |
| | | | | | 1.80 | 506.9 | 193.9 | 219.3 | 0.43 | 1.13 | 1.13 | 168.1 | 0.33 | 0.87 |
| | | | | | 2.15 | 724.2 | 220.8 | 259.8 | 0.36 | 1.18 | 1.18 | 193.6 | 0.27 | 0.88 |
| | | | | | 2.36 | 869.0 | 231.5 | 282.7 | 0.33 | 1.22 | 1.22 | 207.7 | 0.24 | 0.90 |
| | CY | 0.692 | 0.698 | 178.83 | 0.99 | 174.7 | 108.5 | 132.3 | 0.76 | 1.22 | 1.22 | 113.1 | 0.65 | 1.04 |
| | | | | | 1.18 | 248.1 | 138.6 | 162.0 | 0.65 | 1.17 | 1.17 | 133.8 | 0.54 | 0.97 |
| | | | | | 1.47 | 384.4 | 179.1 | 204.5 | 0.53 | 1.14 | 1.14 | 162.3 | 0.42 | 0.91 |
| | | | | | 1.65 | 489.2 | 200.4 | 230.9 | 0.47 | 1.15 | 1.15 | 179.5 | 0.37 | 0.90 |
| | | | | | 1.98 | 698.9 | 236.8 | 274.5 | 0.39 | 1.16 | 1.16 | 207.2 | 0.30 | 0.88 |
| | | | | | 2.17 | 838.7 | 254.0 | 299.0 | 0.36 | 1.18 | 1.18 | 222.6 | 0.27 | 0.88 |

Table A6: Numerical ultimate loads and DSM estimates concerning the columns analyzed at *500* ºC.

| *Column* | $\sigma$-$\varepsilon$ | $k_y$ | $k_E$ | $P_{cr}$ ($kN$) | $\bar{\lambda}_D$ | $P_y$ ($kN$) | $P_u$ ($kN$) | $P_{n.D}$ ($kN$) | $\frac{P_u}{P_y}$ | $\frac{P_{n.D}}{P_y}$ | $\frac{P_{n.D}}{P_u}$ | $P^*_{n.D}$ ($kN$) | $\frac{P^*_{n.D}}{P_y}$ | $\frac{P^*_{n.D}}{P_u}$ |
|---|---|---|---|---|---|---|---|---|---|---|---|---|---|---|
| C130 | EC | 0.780 | 0.600 | 81.58 | 1.30 | 138.5 | 74.5 | 82.5 | 0.54 | 0.60 | 1.11 | 66.8 | 0.48 | 0.90 |
| | | | | | 1.55 | 196.6 | 89.4 | 98.9 | 0.45 | 0.50 | 1.11 | 77.7 | 0.40 | 0.87 |
| | | | | | 1.93 | 304.6 | 102.2 | 122.5 | 0.34 | 0.40 | 1.20 | 92.8 | 0.30 | 0.91 |
| | | | | | 2.18 | 387.7 | 101.5 | 137.2 | 0.26 | 0.35 | 1.35 | 102.1 | 0.26 | 1.01 |
| | | | | | 2.61 | 553.8 | 120.5 | 161.6 | 0.22 | 0.29 | 1.34 | 117.0 | 0.21 | 0.97 |
| | | | | | 2.85 | 664.6 | 155.4 | 175.4 | 0.23 | 0.26 | 1.13 | 125.3 | 0.19 | 0.81 |
| | RM | 0.462 | 0.480 | 65.27 | 1.12 | 82.0 | 51.0 | 55.9 | 0.68 | 1.10 | 1.10 | 46.6 | 0.57 | 0.91 |
| | | | | | 1.34 | 116.4 | 63.2 | 67.7 | 0.58 | 1.07 | 1.07 | 54.6 | 0.47 | 0.86 |
| | | | | | 1.66 | 180.4 | 74.6 | 84.7 | 0.47 | 1.14 | 1.14 | 65.8 | 0.36 | 0.88 |
| | | | | | 1.88 | 229.6 | 78.5 | 95.3 | 0.41 | 1.21 | 1.21 | 72.5 | 0.32 | 0.92 |
| | | | | | 2.24 | 328.0 | 94.8 | 112.7 | 0.34 | 1.19 | 1.19 | 83.4 | 0.25 | 0.88 |
| | | | | | 2.46 | 393.6 | 104.0 | 122.5 | 0.31 | 1.18 | 1.18 | 89.5 | 0.23 | 0.86 |
| | CY | 0.159 | 0.479 | 65.13 | 0.66 | 28.2 | 21.4 | 27.4 | 0.97 | 1.28 | 1.28 | 26.0 | 0.92 | 1.21 |
| | | | | | 0.78 | 40.1 | 25.2 | 35.7 | 0.89 | 1.41 | 1.41 | 32.2 | 0.80 | 1.28 |
| | | | | | 0.98 | 62.1 | 36.3 | 47.5 | 0.76 | 1.31 | 1.31 | 40.7 | 0.66 | 1.12 |
| | | | | | 1.10 | 79.0 | 43.4 | 54.7 | 0.69 | 1.26 | 1.26 | 45.8 | 0.58 | 1.05 |
| | | | | | 1.32 | 112.9 | 55.0 | 66.6 | 0.59 | 1.21 | 1.21 | 53.8 | 0.48 | 0.98 |
| | | | | | 1.44 | 135.5 | 61.6 | 73.2 | 0.54 | 1.19 | 1.19 | 58.3 | 0.43 | 0.95 |
| R135 | EC | 0.780 | 0.600 | 153.73 | 1.13 | 197.0 | 125.2 | 133.2 | 0.68 | 1.06 | 1.06 | 110.8 | 0.56 | 0.89 |
| | | | | | 1.35 | 279.7 | 147.4 | 161.2 | 0.58 | 1.09 | 1.09 | 129.8 | 0.46 | 0.88 |
| | | | | | 1.68 | 433.3 | 180.1 | 201.4 | 0.46 | 1.12 | 1.12 | 156.2 | 0.36 | 0.87 |
| | | | | | 1.89 | 551.5 | 201.1 | 226.5 | 0.41 | 1.13 | 1.13 | 172.2 | 0.31 | 0.86 |
| | | | | | 2.26 | 787.8 | 226.3 | 267.8 | 0.34 | 1.18 | 1.18 | 198.0 | 0.25 | 0.87 |
| | | | | | 2.48 | 945.4 | 234.5 | 291.2 | 0.31 | 1.24 | 1.24 | 212.3 | 0.22 | 0.91 |
| | RM | 0.462 | 0.480 | 122.98 | 0.97 | 116.7 | 82.2 | 89.3 | 0.77 | 1.09 | 1.09 | 76.7 | 0.66 | 0.93 |
| | | | | | 1.16 | 165.7 | 104.5 | 109.6 | 0.66 | 1.05 | 1.05 | 90.7 | 0.55 | 0.87 |
| | | | | | 1.44 | 256.6 | 129.1 | 138.5 | 0.54 | 1.07 | 1.07 | 110.2 | 0.43 | 0.85 |
| | | | | | 1.63 | 326.6 | 141.2 | 156.5 | 0.48 | 1.11 | 1.11 | 121.9 | 0.37 | 0.86 |
| | | | | | 1.95 | 466.6 | 163.1 | 186.1 | 0.40 | 1.14 | 1.14 | 140.8 | 0.30 | 0.86 |
| | | | | | 2.13 | 559.9 | 174.2 | 202.8 | 0.36 | 1.16 | 1.16 | 151.3 | 0.27 | 0.87 |
| | CY | 0.159 | 0.479 | 122.72 | 0.57 | 40.1 | 30.7 | 40.1 | 1.00 | 1.31 | 1.31 | 40.0 | 1.00 | 1.30 |
| | | | | | 0.68 | 57.0 | 38.6 | 54.5 | 0.96 | 1.41 | 1.41 | 51.2 | 0.90 | 1.32 |
| | | | | | 0.85 | 88.3 | 56.4 | 74.8 | 0.85 | 1.33 | 1.33 | 66.2 | 0.75 | 1.17 |
| | | | | | 0.96 | 112.4 | 68.1 | 87.3 | 0.78 | 1.28 | 1.28 | 75.2 | 0.67 | 1.10 |
| | | | | | 1.14 | 160.6 | 88.9 | 107.6 | 0.67 | 1.21 | 1.21 | 89.3 | 0.56 | 1.00 |
| | | | | | 1.25 | 192.7 | 100.1 | 119.0 | 0.62 | 1.19 | 1.19 | 97.1 | 0.50 | 0.97 |

Table A7: Numerical ultimate loads and DSM estimates concerning the columns analyzed at *600* ºC.

| *Column* | $\sigma$-$\varepsilon$ | $k_y$ | $k_E$ | $P_{cr}$ ($kN$) | $\bar{\lambda}_D$ | $P_y$ ($kN$) | $P_u$ ($kN$) | $P_{n.D}$ ($kN$) | $\frac{P_u}{P_y}$ | $\frac{P_{n.D}}{P_y}$ | $\frac{P_{n.D}}{P_u}$ | $P^*_{n.D}$ ($kN$) | $\frac{P^*_{n.D}}{P_y}$ | $\frac{P^*_{n.D}}{P_u}$ |
|---|---|---|---|---|---|---|---|---|---|---|---|---|---|---|
| C130 | EC | 0.470 | 0.310 | 42.15 | 1.41 | 83.4 | 40.8 | 46.2 | 0.49 | 0.55 | 1.13 | 36.9 | 0.44 | 0.90 |
| | | | | | 1.68 | 118.5 | 48.0 | 55.2 | 0.41 | 0.47 | 1.15 | 42.8 | 0.36 | 0.89 |
| | | | | | 2.09 | 183.5 | 56.0 | 68.1 | 0.31 | 0.37 | 1.22 | 51.0 | 0.28 | 0.91 |
| | | | | | 2.35 | 233.6 | 58.2 | 76.1 | 0.25 | 0.33 | 1.31 | 55.9 | 0.24 | 0.96 |
| | | | | | 2.81 | 333.7 | 78.3 | 89.5 | 0.23 | 0.27 | 1.14 | 64.0 | 0.19 | 0.82 |
| | | | | | 3.56 | 533.9 | 86.4 | 110.0 | 0.16 | 0.21 | 1.27 | 76.1 | 0.14 | 0.88 |
| | RM | 0.192 | 0.350 | 47.59 | 0.85 | 34.1 | 25.2 | 28.9 | 0.85 | 1.15 | 1.15 | 25.6 | 0.75 | 1.02 |
| | | | | | 1.01 | 48.4 | 32.6 | 36.1 | 0.74 | 1.11 | 1.11 | 30.7 | 0.63 | 0.94 |
| | | | | | 1.26 | 75.0 | 42.8 | 46.2 | 0.62 | 1.08 | 1.08 | 37.7 | 0.50 | 0.88 |
| | | | | | 1.42 | 95.4 | 48.6 | 52.5 | 0.55 | 1.08 | 1.08 | 41.9 | 0.44 | 0.86 |
| | | | | | 1.69 | 136.3 | 55.2 | 62.9 | 0.46 | 1.14 | 1.14 | 48.7 | 0.36 | 0.88 |
| | | | | | 1.85 | 163.6 | 57.5 | 68.7 | 0.42 | 1.19 | 1.19 | 52.4 | 0.32 | 0.91 |
| | CY | 0.091 | 0.197 | 26.79 | 0.78 | 16.2 | 11.3 | 14.5 | 0.90 | 1.29 | 1.29 | 13.1 | 0.81 | 1.16 |
| | | | | | 0.93 | 22.9 | 13.2 | 18.3 | 0.80 | 1.39 | 1.39 | 15.9 | 0.69 | 1.20 |
| | | | | | 1.15 | 35.5 | 18.5 | 23.7 | 0.67 | 1.28 | 1.28 | 19.6 | 0.55 | 1.06 |
| | | | | | 1.30 | 45.2 | 21.9 | 27.0 | 0.60 | 1.23 | 1.23 | 21.9 | 0.48 | 1.00 |
| | | | | | 1.55 | 64.6 | 26.4 | 32.5 | 0.50 | 1.23 | 1.23 | 25.5 | 0.39 | 0.96 |
| | | | | | 1.70 | 77.5 | 28.7 | 35.6 | 0.46 | 1.24 | 1.24 | 27.5 | 0.35 | 0.96 |
| R135 | EC | 0.470 | 0.310 | 79.43 | 1.22 | 118.7 | 68.1 | 74.9 | 0.63 | 1.10 | 1.10 | 61.4 | 0.52 | 0.90 |
| | | | | | 1.46 | 168.5 | 81.7 | 90.2 | 0.54 | 1.10 | 1.10 | 71.7 | 0.43 | 0.88 |
| | | | | | 1.81 | 261.1 | 97.8 | 112.2 | 0.43 | 1.15 | 1.15 | 85.9 | 0.33 | 0.88 |
| | | | | | 2.05 | 332.3 | 108.5 | 125.9 | 0.38 | 1.16 | 1.16 | 94.5 | 0.28 | 0.87 |
| | | | | | 2.44 | 474.7 | 119.8 | 148.5 | 0.31 | 1.24 | 1.24 | 108.5 | 0.23 | 0.91 |
| | | | | | 2.68 | 569.6 | 122.2 | 161.3 | 0.28 | 1.32 | 1.32 | 116.3 | 0.20 | 0.95 |
| | RM | 0.192 | 0.350 | 89.67 | 0.74 | 48.5 | 37.0 | 44.8 | 0.92 | 1.21 | 1.21 | 41.1 | 0.85 | 1.11 |
| | | | | | 0.88 | 68.8 | 45.3 | 57.0 | 0.83 | 1.26 | 1.26 | 50.1 | 0.73 | 1.11 |
| | | | | | 1.09 | 106.7 | 72.0 | 74.5 | 0.70 | 1.03 | 1.03 | 62.4 | 0.59 | 0.87 |
| | | | | | 1.23 | 135.7 | 81.1 | 85.2 | 0.63 | 1.05 | 1.05 | 69.8 | 0.51 | 0.86 |
| | | | | | 1.47 | 193.9 | 94.7 | 102.9 | 0.53 | 1.09 | 1.09 | 81.6 | 0.42 | 0.86 |
| | | | | | 1.61 | 232.7 | 102.1 | 112.8 | 0.48 | 1.10 | 1.10 | 88.1 | 0.38 | 0.86 |
| | CY | 0.091 | 0.197 | 50.47 | 0.67 | 23.0 | 17.2 | 22.1 | 0.96 | 1.29 | 1.29 | 20.8 | 0.90 | 1.21 |
| | | | | | 0.80 | 32.6 | 21.9 | 28.6 | 0.88 | 1.31 | 1.31 | 25.7 | 0.79 | 1.17 |
| | | | | | 1.00 | 50.6 | 29.3 | 37.9 | 0.75 | 1.29 | 1.29 | 32.3 | 0.64 | 1.10 |
| | | | | | 1.13 | 64.3 | 34.8 | 43.6 | 0.68 | 1.25 | 1.25 | 36.3 | 0.56 | 1.04 |
| | | | | | 1.35 | 91.9 | 44.0 | 53.0 | 0.58 | 1.20 | 1.20 | 42.6 | 0.46 | 0.97 |
| | | | | | 1.48 | 110.3 | 50.6 | 58.2 | 0.53 | 1.15 | 1.15 | 46.1 | 0.42 | 0.91 |